REPORT No. 90

CONDENSATION OF SUPERSATURATED ORGANIC VAPORS IN A SUPERSONIC NOZZLE

Daniel B. Dawson

Research was carried out under the Sponsorship of the U. S. Navy, Office of Naval Research, Power Branch
Contract Nonr 3963(07)

April, 1967

GAS TURBINE LABORATORY
MASSACHUSETTS INSTITUTE OF TECHNOLOGY
CAMBRIDGE · 39 · MASSACHUSETTS

CONDENSATION OF SUPERSATURATED ORGANIC VAPORS IN A SUPERSONIC NOZZLE

by

DANIEL B. DAWSON

Research was carried out under the
Sponsorship of the U. S. Navy, Office
of Naval Research, Power Branch
Contract Nonr 3963(07)

GAS TURBINE LABORATORY

REPORT No. 90

April 1967

MASSACHUSETTS INSTITUTE OF TECHNOLOGY

Cambridge, Massachusetts

ABSTRACT

Experiments were performed involving condensation of supersaturated benzene and chloroform vapors in a supersonic nozzle, with compressed air as the carrier gas.

Measurements were made by means of static pressure taps along the nozzle walls, and from the resultant pressure profile it was possible to deduce the point of incidence of condensation. Incidence of condensation for chloroform was generally above the triple point, whereas incidence for benzene was generally below the triple point. For the latter, condensate droplets were assumed to be supercooled liquid, and physical properties for these droplets were obtained from the extrapolation of liquid properties.

Experiments showed that the magnitude of the water vapor content of the carrier air made no observable difference in the condensation behavior of either fluid. It was demonstrated that addition of small amounts of these fluids to the carrier air tended to reduce the thickness of the boundary layer in the nozzle.

Comparison of experimental results with theory show, without making any adjustments to physical properties of condensate droplets to account for size, that incidence of condensation for chloroform can be predicted by the revised theory of nucleation, whereas benzene incidence can be predicted by neither revised nor classical theory. These results, combined with prior data on other fluids, show that at present neither theory seems to be generally applicable. In support of previous conclusions, the problem may well be the assumption that bulk properties may be assigned to small (30 - 50 molecules) droplets of condensate.

ACKNOWLEDGEMENTS

The author is indebted to his thesis advisor, Professor K. C. Russell of the Department of Metallurgy, for his advice and guidance throughout the period during which this work was in progress. His contributions to the theoretical considerations were appreciated, as were his efforts to maintain the relationship of this project to the field of metallurgy.

The author further wishes to express his gratitude for the assistance, encouragement, and advice of Professor P. G. Hill of the Department of Mechanical Engineering, who originated the condensation work undertaken at the Gas Turbine Laboratory, and acted as unofficial advisor for this experiment.

Mr. Harry Jaeger spent considerable time demonstrating the apparatus and assisting with matters of theory and procedure, and his earlier work provides the basis on which this report is built. Mr. Ernest Willson made or modified much of the existing equipment, and helped with the running of the early experiments. Mr. Thorvald Christensen was likewise instrumental in the manufacture and setup of the experimental apparatus.

Mrs. Joan Kukolich provided assistance with theoretical problems as well as doing much of the programming. Mrs. Madelyn Euvrard, prior to a temporary leave necessitated by illness, was helpful in the procurement of supplies and equipment, and in making the author feel at home in the G.T.L. Miss Jennifer Jacobs typed the final draft of the manuscript, managing text, equations and corrections in excellent humor.

Finally, the author wishes to thank his wife, Betty, who has combined the roles of wage earner, manuscript typist, and mother-to-be, and provided the encouragement necessary to complete this project.

TABLE OF CONTENTS

	Page
ABSTRACT	i
ACKNOWLEDGEMENTS	ii
TABLE OF CONTENTS	iii
LIST OF FIGURES	v
NOMENCLATURE	vi
I. INTRODUCTION	1
I.A Background to the Problem	1
I.B Earlier Investigations	2
I.C The Present Experiment	4
II. EXPERIMENTAL PROGRAM	6
II.A Preliminary Considerations	6
II.B Experimental Equipment	10
II.C Experimental Procedure	14
II.D Presentation of Data	15
III. THEORETICAL CONSIDERATIONS	18
III.A Gas Dynamics	18
III.B Nucleation Theory	19
III.C Drop Growth	23
IV. COMPARISON OF THEORY WITH EXPERIMENTAL DATA	26
IV.A Incidence of Condensation	26
IV.B Pressure Profile Shape	28
V. CONCLUSIONS	30
TABLE I - SUMMARY OF BENZENE EXPERIMENTS AND RESULTS	32

	Page
TABLE II - SUMMARY OF CHLOROFORM EXPERIMENTS AND RESULTS	34
REFERENCES	35
FIGURES 1-15	
APPENDIX A - METERING OF THE INJECTED VAPOR	A-1
APPENDIX B - CALCULATION OF ω_o AND y_o	B-1
APPENDIX C - DERIVATION OF GAS DYNAMIC RELATIONS	C-1
APPENDIX D - EFFECT OF PRESSURE, MOISTURE AND INJECTED VAPOR ON EFFECTIVE NOZZLE FLOW AREA	D-1
APPENDIX E - CALCULATION OF PHYSICAL AND THERMODYNAMIC PROPERTIES OF THE TEST FLUIDS	E-1
APPENDIX F - TABULATION OF EXPERIMENTAL DATA	F-1

LIST OF FIGURES

1. Schematic Diagram of Apparatus.

2. Detail of Nozzle II.

3. Effective Area Distribution of Nozzle II.

4. Mass-Flow Effect on Pressure Profiles with Benzene Condensation, Tests 9, 15 and 19.

5. Temperature Effect on Pressure Profiles with Benzene Condensation, Tests 19 and 34.

6. Comparison of Theory with Data for Benzene Condensation, Test 12.

7. Comparison of Theory with Data for Benzene Condensation, Test 10.

8a. Comparison of Theory with Data for Benzene Condensation, Test 23.

8b. Effect of Decrease in Surface Tension, Test 23.

8c. Effect of Increase in Surface Tension, Test 23.

9. Incidence of Benzene Condensation.

10. Mass-Flow Effect on Pressure Profiles with Chloroform Condensation, Tests 54 and 67.

11. Temperature Effect on Pressure Profiles with Chloroform Condensation, Tests 61 and 66.

12. Comparison of Theory with Data for Chloroform Condensation, Test 46.

13. Comparison of Theory with Data for Chloroform Condensation, Test 48.

14. Comparison of Theory with Data for Chloroform Condensation, Test 49.

15. Incidence of Chloroform Condensation.

NOMENCLATURE

A	Nozzle flow area
A^*	Nozzle flow area at throat
C	Pre-exponential factor in nucleation-rate equation
c_L	Specific heat of condensate
c_p	Specific heat of perfect gas at constant pressure
c'_p	Specific heat at constant pressure of mixture of carrier and vapor
c_v	Specific heat of perfect gas at constant volume
g^*	Number of molecules in critical-sized cluster
ΔG^*	Free energy of formation of critical-sized cluster
$\Delta G^{*'}$	Free energy of formation of critical-sized cluster without gasification effects
h_f	Specific enthalpy of condensate
h_{fg}	Latent heat of vaporization
J	Nucleation rate, nuclei per unit time per unit volume
K	Boltzmann Gas Constant
K	Shape factor in calculating droplet surface area
M	Mach number
$\bar{M}$	Molecular weight
$\dot{m}$	Mass-flow rate
$\bar{m}$	Mass of molecule
P	Stream pressure
p	Vapor pressure
R	Gas constant
$\bar{R}$	Universal gas constant
r	Radius of droplet

r^*	Radius of critical-sized droplets
$\bar{r}$	Surface-area average radius
S	Supersaturation ratio, p/p_{sat}
T	Temperature
U_f	Internal energy of condensate
u	Stream velocity
v	Specific volume
v_L	Volume per molecule of liquid phase
x	Streamwize co-ordinate
y	Mole fraction of injected vapor
Z	A function of γ, $Z = 1/(\gamma-1) + 1/2$
β	Mass flux impinging on droplet surface
Γ	Gasification factor in nucleation-rate equation
γ	Ratio of specific heats, c_p/c_v
μ	Mass fraction of stream that is condensate
ξ	Condensation coefficient
ρ	Density
σ	Surface tension
ω	Mass fraction of stream that is injected vapor

Subscripts

c	Referring to the carrier gas
D	Referring to the droplet conditions
i	Referring to conditions at incidence of condensation
L	Referring to the liquid state
m	Referring to the carrier gas + vapor mixture
$^\circ$	Referring to initial or stagnation conditions

s	Referring to the solid state
v	Referring to the vapor
∞	Referring to conditions at the flat-film equilibrium state

I. INTRODUCTION

A. Background to the Problem

Despite the considerable amount of recent experimentation that has been done on the subject of homogeneous nucleation and growth of condensate droplets from a supersaturated vapor, much work yet remains to be done.

An understanding of the nature of condensation is of prime importance in many fields, particularly in the design of steam turbines. Condensate droplets can erode turbine components severely, and condensation may result in the failure of the turbine to achieve predicted performance if it is not taken into account in design calculations. With the possibility that in the near future turbines may be run using metal vapors as the working fluid, it is imperative that condensation studies be extended to a larger range of materials. While it is of course desirable to ascertain in detail the condensation behavior of certain fluids with particular applications, it is also desirable (and perhaps necessary) that knowledge of the theoretical aspects of nucleation and growth processes be advanced at the same time. In particular, many fluids do not, for a variety of reasons, lend themselves to the study of their condensation behavior. In such cases, accurate and applicable theoretical prediction of the condensation process would be invaluable.

Advances in the understanding of nucleation and growth have applications in other fields, also. Metallurgy and ceramics, for instance, deal with phase changes of a different nature; mainly liquid-solid (solidification) and solid-solid. However, the nucleation and growth equations for these

transformations are in many cases either identical to or similar to the corresponding condensation equations. But the study of vapor-liquid transformations has an advantage in that both the experiments and the theoretical relations are simpler than in the case of liquid-solid and solid-solid transformations.

B. Earlier Investigations

The earliest condensation experiments were performed in cloud chamber apparatus. Experiments by Wilson (1899) and Powell (1928) were followed by work with a number of fluids by Volmer and Flood (1934). The cloud chamber method has certain drawbacks, however. For one thing, the onset of condensation is chosen as the point at which a cloud first becomes visible. This depends to a large degree on the judgment of a particular observer, and the appearance of a cloud may correspond to a time considerably later than the onset of substantial nucleation. Also, the slow rate of expansion in the cloud chamber means that much care must be taken that foreign particles (such as dust) are not present in any large quantities, or homogeneous nucleation will not be possible. Finally, the observations are qualitative rather than quantitative.

These objections are largely done away with by conducting the expansion in a converging-diverging supersonic nozzle. The expansion is rapid enough that, as demonstrated by Stodola (1927) and others, homogeneous nucleation should occur even for high concentrations of dust particles. And, the condensation process may be observed down the length of the nozzle by pressure measurements.

A considerable number of nozzle experiments have been conducted using steam or water vapor as the working fluid, which is understandable when one

considers the importance of the steam turbine in industry today. Among the experimenters have been Yellot (1934), Rettaliata (1936), Binnie and Woods (1938), Binnie and Green (1942), and more recently Wegener and Pouring (1964) and Jaeger (1966). Water vapor, however, is certainly not an ideal fluid for the study of nucleation and growth, since its behavior is influenced to a large degree by the high dipole moment of the water molecule.

Data on other fluids is limited. Stever and Rathbun (1951) studied condensation of air, and Willmarth and Nagamatsu (1952) and Faro, Small and Hill (1952) provide some data on nitrogen. Scharrer (1939) studied the nucleation on ions of several organic fluids. Tests in the Gas Turbine Laboratory have been conducted recently by Duff (1966) using pure carbon dioxide, by Kremmer and Okurounmu (1965) using pure ammonia, and by Jaeger (1966) using ammonia and water vapor mixed with air used as a carrier gas.

Reviews of existing data have been made by Wegener (1958), Stever (1958) and Hill (1965). There have been efforts in these and other papers to find some correlation between experimental data and the present theoretical equations for nucleation and growth.

At present there are two conflicting theories concerning the nucleation of condensate from the supersaturated vapor. One approach, usually referred to as the classical theory, treats the condensate nuclei as stationary in space. Lothe and Pound (1962) and others have proposed a revised theory in which the partition functions for the rotational and translational degrees of freedom of the nuclei are accounted for, resulting in a substantial increase in predicted nucleation rate. For the tests conducted here using benzene and chloroform, the rates predicted by revised theory were on the order of 10^{15} greater than those predicted by classical theory.

By means of laborious hand calculations, Oswatitsch (1942) was able to show for a limited amount of data that water vapor condensation agreed well with the predictions of classical theory. This was confirmed by Hill (1965) and Jaeger (1966) using a procedure involving the IBM 7094 computer. With the assumption that supercooled liquid nuclei exist below the triple point, the data of Duff (1966) on carbon dioxide also agrees well with the classical nucleation equations. On the other hand, Kremmer and Okurounmu (1965) and Jaeger (1966) conclude that ammonia shows much better agreement with the revised theory.

C. The Present Experiment

The experiments detailed herein were undertaken to expand the previous Gas Turbine Laboratory condensation work to include two more liquids. The nozzle used here was used in all three previous Gas Turbine Laboratory investigations, and the other experimental equipment was identical in most respects to that used by Jaeger (1966).

There are, of course, both advantages and disadvantages to using similar equipment. On the positive side, many of the problems which one ordinarily encounters in assembling experimental apparatus have been ironed out. Furthermore, additional investigations may provide support for previous work or corrections for previous mistakes. On the other hand, there is a tendency to perpetuate these same mistakes. For this and other reasons, it is desirable that experiments be conducted with the same fluids but on different apparatus, so as to provide a check on the work conducted here.

Benzene and chloroform were chosen as test fluids for several reasons. It was hoped that experimental data on them would provide some resolution of the conflict over nucleation theories. As will be discussed in Section II,

each fluid had certain properties which governed its choice.

The results of the tests were certainly not in uniform support of either of the theories. It is true that chloroform agreed well with the revised theory. But benzene did not agree with either revised or classical theory. In fact, results for benzene indicated that a nucleation rate approximately midway between the two theories (or about a factor 10^8 times the rate predicted by classical theory) provided generally good agreement between data and theory. This conflicting data seems best to support the conclusion of Jaeger (1966) that any agreement between data and the present theories is mostly fortuitous.

II. EXPERIMENTAL PROGRAM

A. Preliminary Considerations

It has already been mentioned that one of the chief problems encountered with the cloud chamber apparatus is that of ensuring that nucleation is homogeneous, rather than heterogeneous. The presence of sites on which nuclei will preferentially form will reduce the supersaturation necessary to cause condensation if these sites are present in sufficient quantities. In an expansion in a supersonic nozzle, the problem of contamination due to the presence of heterogeneous nucleation sites is not as serious as it is in the case of the cloud chamber, principally because the expansion rate (and hence the nucleation rate) is much greater in the nozzle.

The contamination can be of three principal types: dust and other inert foreign particles, water vapor, and liquid droplets of the test vapor present prior to the incidence of condensation.

It is shown in calculations by Duff (1966) that there is little chance that dust particles could be present in concentrations sufficient to make homogeneous nucleation difficult. However, in the experiments run here, the carrier air was filtered as a precaution, and prior to any actual measurements the apparatus was always run for a few minutes to clear out any dust which might have accumulated in the pipes.

Jaeger (1966) showed that the presence of water vapor had a significant effect on the critical supersaturation necessary for condensation of ammonia. This was to be expected since ammonia has an affinity for water vapor. For benzene and chloroform, no such effect would be expected. However, to check this assumption, some tests were run in which the moisture present in the

carrier air was reduced from a normal concentration of 35 parts per million (by weight) to less than .03 parts per million.

The presence of liquid droplets mixed with vapor prior to condensation was a more serious problem than the two previously mentioned. This would arise if the liquid benzene or chloroform were not vaporized completely before being injected into the carrier air stream. As a result, the mass fraction of injected vapor would be overestimated, and the liquid droplets would provide heterogeneous nucleation sites. As will be described, a means of visually checking the extent of vaporization was installed at the vapor injection point.

A point which needed checking was the assumption made previously by Jaeger (1966) that the thickness of the boundary layer at any position in the nozzle was unchanged either by the injection of a vapor into the carrier air stream, or by small pressure changes due to condensation or variation of stagnation pressure. The investigation of these effects is considered in more detail in Appendix D.

The choice of benzene and chloroform for these tests was dictated by several factors. Most previous nozzle work had been done on relatively light molecules (carbon dioxide, with a molecular weight of 48, being the heaviest), so it was desirable to extend the experiments to heavier molecules. Also, because the effect of the molecular dipole moment on condensation behavior has not been resolved, benzene (with a zero moment) proved to be an interesting fluid to study. Chloroform had the advantage of a low freezing point. Since expansion in the nozzle was unlikely to cool the fluid below this point, there was no need to decide whether to assume solid or supercooled liquid chloroform below the triple point. This problem arose

with other fluids, including benzene, where the triple point was higher. Toxicity was a problem with both fluids, but was not the problem it might have been for other fluids (such as carbon tetrachloride). Finally, there had to be sufficient data available in the literature that the physical properties of these fluids could be found over a wide range of temperatures.

Another consideration was the selection of the most useful experimental technique for studying the condensation process. Duff (1966) found interferometry to be useful in showing that flow was one-dimensional and in investigating the boundary layer thickness at the nozzle throat, but had no success in applying the same method to condensation. Jaeger (1966) studied the normal shock characteristic in condensing flow and concluded that any possible advantages that this method might have were far outweighed by inherent disadvantages.

In view of the good results obtained by most previous investigators when using static pressure measurements, this method was adopted for all tests. As a means for studying condensation, it has several advantages. It gives a quantitative rather than qualitative measure of condensation, and the measurements by static pressure taps are easily taken and easy to interpret. The static pressure at any distance from the nozzle throat gives a continuous measure of the effect of condensation by the relation (to be derived later):

$$\frac{1}{P}\frac{dP}{dx} = \left[\frac{\gamma M^2}{(M^2-1)(1-\mu) + \mu\gamma M^2}\right]\left[\left(\frac{h_{fg}}{C_p T} - \frac{1}{(1-\omega_o)\bar{M}_v/\bar{M}_c + \omega_o - \mu}\right)\frac{d\mu}{dx} - \frac{1}{A}\frac{dA}{dx}\right] \qquad (1)$$

where P is the static pressure

M is the Mach number

μ is the mass fraction of the total mass flow that has condensed

γ is the specific heat ratio (C_p/C_v) of the uncondensed gas mixture

h_{fg} is the latent heat vaporization of the test vapor

C_p is the specific heat of the uncondensed gas mixture

T is the absolute temperature

$(1-\omega_b)$ is the mass fraction of the total mass flow that is carrier air

$\bar{M}_v, \bar{M}_c$ are the molecular weights of the test vapor and carrier air, respectively

A is the flow area

x is the distance from the nozzle throat

Note that when $\mu = d\mu = 0$, the relation reduces to the expression for an isentropic expansion. When condensation occurs and μ and $d\mu$ are not 0, there will be a rise in pressure if the first term of the $d\mu/dx$ coefficient (due to the release of latent heat) is greater than the second term.

Note, also, that the second term of the $d\mu/dx$ expression approaches a value of $1/(1-\mu)$ when the molecular weight of the test vapor is close to the molecular weight of the carrier air (=29). In this case, for a pressure rise to occur we must have:

$$\frac{h_{fg}}{C_p T} > \frac{1}{1-\mu} \approx 1 \qquad \text{(since } \mu \text{ is generally less than 0.25)}$$

In the case of benzene ($\bar{M}_v$ = 78.1) and chloroform ($\bar{M}_v$ = 119.4), the second term becomes much smaller; on the order of 0.4 and 0.3 respectively. As a result, the latent heat term does not have to be very large in order to get a substantial pressure increase due to condensation.

Another point to consider is that as the condensation occurs closer to the throat (and hence the Mach number approaches 1.0), the denominator

in the first term on the right-hand side of equation (1) becomes very small, and therefore the magnitude of any pressure rise which may occur due to condensation will become much greater.

B. Experimental Equipment

The equipment used in this experiment may be divided into three broad categories. There is a system to provide high pressure carrier air. There is a second system to store, meter, and vaporize measured quantities of the test liquid, and to mix this vapor with the carrier air. Finally, there is the nozzle in which the pressure distribution is measured. A schematic drawing of the test equipment is given as Figure 1.

1. Carrier Air System

The carrier air was supplied by an oil-free, two-stage, piston-type compressor. A large receiving tank maintained a steady supply of the air at 90 psig. After leaving the tank, the air was filtered twice, and then dried in a dehumidifier. The dehumidifier was packed with activated alumina desiccant, and if properly reactivated after prior use, it could provide dried air with a dewpoint of -60°F (which, at one atmosphere total pressure, corresponds to 35 ppm water vapor if one assumes extrapolated liquid properties below the triple point). Because of dehumidifier limitations, the pressure available was reduced to 60 psig by means of a regulator on the air line.

Further drying of the air could be accomplished by the use of a cold trap. This was, in essence, a counterflow heat exchanger with one end immersed in boiling liquid nitrogen (-321°F), so that air passing through the low temperature end would lose most of the water vapor present. Taking air from the dehumidifier at a dew point of -60°F, the cold trap could reduce

the moisture content to a dew point of less than -150° F (corresponding to .03 ppm water), which was the lowest limit which could be measured by the available equipment. The counterflow arrangment allowed nearly total temperature recovery of the carrier air at exit. The cold trap could be used without any liquid nitrogen if a moisture level lower than that provided by the dehumidifier was not necessary, or (as shown in the schematic) it could be bypassed entirely. The pressure drop in the cold trap was about 5 psi greater than when the bypass was used.

After passing through the cold trap, the carrier air could be heated in another heat exchanger. This consisted of a stainless-steel coil (through which the air passed) contained in a jacket through which steam could be passed. It was used in only about half of the experiments, primarily when a fixed temperature was desired. Stagnation temperatures of over 200° F could be obtained with this heater, but the use of lucite view port windows on the air line made such high temperatures dangerous.

To measure the moisture content of the carrier air, an "Alnor Dew Pointer" was connected to a tap on the air line downstream of the point of test vapor injection (the reason for the choice of this position will be discussed later). This device operates on the cloud chamber principle. A sample of air is expanded rapidly into a chamber, and will show a condensation cloud if the expansion is great enough. The dew point is related to the expansion ratio at which a cloud is first visible, and precise instructions for obtaining it are given with the "Dew Pointer". The device was never operated when benzene or chloroform were being injected into the carrier air, since these liquids would have a disastrous effect on any rubber gaskets or seals present.

2. Test Vapor Injection System

The liquid was stored in a pressurized tank, and metered with a flat-plate orifice. This equipment is described in more detail in Appendix A.

The stream of liquid passing through the metering orifice was heated in two heat exchangers before being injected into the carrier air system as vapor. The first was three feet long, of the counterflow type, and heated with high pressure (120 psig) steam. The second consisted of a coiled fifteen-foot length of 1/4" diameter stainless steel tubing, wrapped with electrical heating tape and heated to about 400°F.

To improve the performance of the heat exchangers and assure complete vaporization of the liquid, it was necessary to inject a small quantity of high pressure bleed air downstream of the metering orifice but before the first heat exchanger. Initially, the bleed air was taken directly from the compressor, but the high moisture level of this bleed air negated the drying effect of the cold trap in spite of the small flow rate of air involved. Therefore, the bleed air was subsequently taken immediately upstream of the cold trap, with the pressure drop in the trap providing a sufficient pressure difference to get good heat exchanger performance. Placing the "Dew Pointer" downstream of the vapor injection point, it now proved possible to get dew points of at least -150°F (the lowest that could be measured with the "Dew Pointer"), despite the addition of small amounts of -60°F dew point bleed air.

Propelled by the bleed air, the vaporized test liquid was injected into the two-inch diameter carrier air pipe by a short length of stainless steel tubing which directed the vapor against the pipe wall. At this point, view ports were installed which allowed a visual check on the extent of vaporization. Incomplete vaporization resulted in the pipe wall being wetted

at the injection point. The flow of bleed air was adjusted to the minimum which would still maintain complete vaporization.

3. Nozzle and Related Equipment

The nozzle used was the same one used by Kremmer and Okurounmu (1965), Duff (1966) and Jaeger (1966), and was referred to as Nozzle II by them. Figure 2 shows its construction. It had a rectangular, constant-width cross-section, .15" by .20" wide at the throat. The top and bottom plates were hinged to give a variable divergence angle. In all tests conducted here, the plates were set at a total included angle of about 6°. The side walls were formed by two flat plates, one of which was pierced on the nozzle centerline with .020" diameter static pressure taps, spaced .10" apart in the region in which experimental observations were made, and .20" apart farther downstream. These taps were connected to a manometer board (described below).

The experimentally-determined effective area distribution of Nozzle II is shown in Figure 3. The effective area, or actual flow area, is given by the true area at a given cross section less the area of the boundary layer. More is said about this in Section II.C "Experimental Procedures" and in Appendix D.

Connected to the downstream end of the nozzle was a steam ejector which had the dual purpose of ejecting the toxic benzene and chloroform vapors to the roof, and lowering the back pressure on the nozzle so as to keep the recovery shock far down the nozzle.

The manometer board mentioned previously consisted of a bank of twenty-five mercury-filled, U-tube manometers, each side of the tubes being 100" tall. Nineteen pressure taps on the nozzle were connected to U-tubes, and the pressure distribution which showed on the manometer board could be

photographed instantaneously with a Polaroid camera.

C. Experimental Procedure

The general procedure involved in an experimental run was to first measure the conditions at nozzle inlet: P_o and T_o, the stagnation pressure and temperature; and ω_o, the initial fraction of the total mass flow that was test vapor. Secondly, the pressure distribution in the nozzle was recorded by a Polaroid photograph of the manometer board.

The stagnation pressure near the nozzle inlet, where the Mach number was on the order of 0.1, was measured by a static pressure tap connected to a mercury-filled, U-tube manometer. The stagnation temperature was measured at the same point by an iron-constantin thermocouple placed in the air stream. The mass flow rate of vapor injected into the carrier air could be determined as outlined in Appendix A, and from this the initial mass fraction of vapor, ω_o, could be found by the procedure outlined in Appendix B.

Plotting the distribution of static pressure rations, P/P_o, versus $(A/A^*)_{eff}$, the effective area distribution, has proven to be one of the most useful methods of presenting condensation data. The pressure ratios can be found from the static pressure distribution recorded on the manometer board and the measured stagnation pressure. However, each pressure ratio must be related to a corresponding effective area ratio. This may be done quite easily if we assume that the boundary layer thickness (and hence the effective area ratio) at a given point in the nozzle will not be changed

a) by a change in the composition of the gas mixture, or

b) by small (10 to 20%) variations in the pressure.

As shown in Appendix D, these assumptions are incorrect, but the magnitude of the corrections is small enough that we may, for the time being, ignore them.

With the assumption of an invariant effective area distribution, we need only determine it for one set of conditions. This is most easily done by finding the pressure distribution corresponding to the expansion of pure carrier air in the nozzle.

According to Shapiro (1953), by assuming a one-dimensional, isentropic expansion of a perfect gas we may relate the effective area ratio to the pressure ratio by this equation:

$$A/A^* = \left[\frac{\gamma-1}{2} \left(\frac{2}{\gamma+1} \right)^{(\gamma+1)/(\gamma-1)} \right]^{1/2} (P/P_o)^{-1/\gamma} \left[1 - (P/P_o)^{(\gamma-1)/\gamma} \right]^{-1/2} \qquad (2)$$

This relation is tabulated for various values of γ in the Gas Tables (Keenan and Kaye, 1945). For expansion of pure carrier air, the table for $\gamma = 1.4$ may be used.

With the addition of benzene and chloroform, both of which have a $\gamma = 1.1$, the γ_m of the mixture of carrier air and test vapor will be somewhat less than 1.4. Thus, from equation (2), we find that the pressure ratio for a given area ratio will be somewhat greater for the mixture than for pure air, even for a non-condensing, isentropic expansion.

For an experimental run, the actual pressure ratio corresponding to a given tap will be greater than what would be predicted by the equation (2), the difference being due to the release of latent heat of vaporization upon condensation of the injected vapor as shown by equation (1).

D. Presentation of Data

Two parameters, which represent important means of presenting condensation data, should be explained at this point.

The "supersaturation", or supersaturation ratio, of a vapor is defined as $S = p/p_{sat}$, where p is the actual vapor pressure and p_{sat} is the partial

pressure of saturated vapor at the same temperature. For S<1 the vapor is said to be undersaturated; for S>1 it is supersaturated. S_i, the supersaturation at the onset (or incidence) of condensation, is a useful measure of the condensation behavior of a particular fluid.

The "incidence of condensation" represents the point at which condensation can first be seen to have begun. It generally corresponds to the formation of about 0.1% condensate (by weight), which also corresponds roughly to the first point at which the pressure ratio becomes noticeably greater than the value predicted by equation (2). The point of incidence is defined by the partial pressure, p_i, and temperature, T_i, at which condensation begins.

For a given test, the supersaturation, pressure and temperature at incidence may all be found from the pressure profile by picking the pressure ratio $(P/P_o)_i$ at which the experimental profile first appears to depart significantly from the calculated isentropic expansion profile.

$$P_i = P_o\left(\frac{P}{P_o}\right)_i \qquad \text{and} \qquad p_i = y_o P_i$$

$$T_i = T_o\left(\frac{T}{T_o}\right)_i = T_o\left(\frac{P}{P_o}\right)_i^{(\gamma_m-1)/\gamma_m}$$

where γ_m is the specific heat ratio of the gas mixture, and corresponds to the γ used in equation (2) to calculate the non-condensing profile, and y_o is the initial mole fraction of test vapor at the nozzle inlet. The method of calculation of γ_m and y_o from measured data is given in Appendix B.

The experimental data for all tests is summarized in Tables 1 and 2 for benzene and chloroform, respectively, and includes the following:

a) the initial conditions: ω_o, y_o, P_o, T_o

b) the conditions at incidence of condensation: p_i, T_i, S_i

c) the moisture content of the carrier air, by dew point.

The experimental pressure distributions for all tests are tabulated in Appendix F. Typical pressure distributions, P/P_o versus A/A^*, are shown in Figures 4 through 8 (for benzene), and 10 through 14 (for chloroform).

In Figures 9 and 15, the points of incidence for the benzene and chloroform tests, respectively, are shown along with the corresponding saturation lines on a log-log plot of vapor pressure versus temperature.

Firgures 4 and 10 illustrate the effect of injecting increasing quantities of vapor. If the initial temperature is the same, there will be an increase in the pressure rise due to condensation (a larger "hump", in other words) as well as a rise in the pressure ratio at which the incidence of condensation occurs. Figures 5 and 11 illustrate the effect of increasing the initial temperature. If the mass fraction of injected vapor remains constant, a rise in initial temperature will depress the pressure ratio at which incidence occurs.

Figures 6 through 8 and 12 through 14 show a comparison of theoretical pressure profiles with certain experimental profiles. The methods by which these theoretical profiles may be determined are presented in the following section.

III. THEORETICAL CONSIDERATIONS

The differential equations from which the state of a condensing flow can be derived for any position in the nozzle are based on the theories of gas dynamics, and nucleation and growth of condensed phases. Gas dynamic theory provides three differential equations in terms of four unknowns. The final relation, which makes the solution of the differential equations possible, is obtained from nucleation and growth theory. The method by which the differential equations are derived is outlined below. References are given for those who desire a more detailed derivation.

A. Gas Dynamics

The derivation of the differential equations from gas dynamic theory makes use of the following assumptions:

1. Flow is steady, one-dimensional, and inviscid, and no heat transfer takes place between the fluid and the surroundings.
2. The vapor phase consists of a mixture of perfect gases.
3. The volume of the condensate is negligible in comparison to the volume it occupied as a vapor.
4. The boundary layer thickness (and hence the effective area distribution) is not affected by small changes in pressure, or by a small change in the composition of the vapor phase.

The differential equations were derived from four relations:

1. Conservation of Mass: $\dot{m} = \frac{\rho A u}{1-\mu} = \text{constant}$
2. Conservation of Energy: $C_p dT + u du = h_{fg}\, d\mu$
3. Conservation of Momentum: $-A dP = \dot{m} du$
4. Equation of State for a Perfect Gas: $P = \rho RT$

An additional relationship is found in the definition of the Mach number, $M \equiv u/(\gamma RT)^{1/2}$. As outlined in Appendix C, from these relations

it is possible to obtain three equations (for dP/dx, dT/dx and du/dx) in terms of five unknowns: $P(x)$, $T(x)$, $u(x)$, $\mu(x)$ and $A(x)$.

One of the unknowns, $A(x)$, may be determined from the experimental effective area distribution. One more relation is needed to solve the equations, and this comes from the theory of nucleation and growth of condensed phases.

B. Nucleation Theory

The formation of a condensed phase from the vapor phase is opposed by a potential barrier, the Gibbs Free Energy change (ΔG), which is a function of the size and shape of the condensate particles formed as well as the physical properties of the fluid.

If we assume that the condensate forms spherical droplets (or nuclei), ΔG will reach a maximum value at some droplet radius r^*, called the critical radius, and thereafter will rapidly become smaller. Nuclei whose radii are less than r^* will tend to shrink, and nuclei whose radii are greater than r^* will tend to grow. Thus, ΔG^*, the Gibbs Free Energy of formation of a nucleus of critical radius r^*, represents the potential barrier which opposes the formation of stable condensate droplets.

At present there are two opposing theories which attempt to describe the nucleation process. However, although the two theories disagree on other points, they do agree on the form of the nucleation rate equation:

$$J = C \exp(-\Delta G^*/KT) \tag{3}$$

where
- J is the nucleation rate, in particles per unit volume per unit time, of critical-sized nuclei, at a given point;
- C is a factor to be explained subsequently
- K is the Boltzmann gas constant
- T is the absolute stream temperature

ΔG^* is the total Gibbs Free Energy change in forming a critical-sized nucleus of condensate.

The point of disagreement between the two theories involves the terms which are thought to be contained in ΔG^*.

Classical nucleation theory, as proposed by Becker and Doring (1935), Frenkel (1946), and Zeldovich (1942) among others, makes the assumption that nuclei are stationary in space, and hence the terms involved in ΔG^* may be reduced to two:

1. The change in free energy associated with the formation of the droplet surface;

2. The free energy change due to the isothermal change in vapor pressure which occurs when the vapor condenses as liquid.

The two terms, when combined, may be referred to as $\Delta G^{*'}$ (which may or may not be the total free energy change, ΔG^*, as we shall see).

$$\Delta G^{*'} = -g^* KT\ell n(S) + 4\,(r^*)^2\sigma \qquad (4)$$

where g^* is the number of molecules in a critical-sized cluster

S is the supersaturation

σ is the flat-film surface tension of the liquid in the presence of its own vapor.

The means by which g^* and r^* may be calculated will be shown subsequently, but first, it is necessary to consider the differences in ΔG^* which arise due to the revised nucleation theory.

The revised theory, which was first clearly set forth by Lothe and Pound (1962), and was elaborated upon in Feder, Russell, Lothe and Pound (1966), takes issue with the assumption that nuclei are stationary in space. According to revised theory, one cannot ignore the rotational and translational degrees of freedom present in a nucleus of condensate

in the vapor phase. The total ΔG^* predicted by the revised theory will consist of the $\Delta G^{*'}$ which classical theory predicts, plus free energy contributions from the translational and rotational motion of the droplet as a whole, plus minor correction terms which account for the conservation of degrees of freedom.

Using the notation of Lothe and Pound, the total free energy change may be written as:

$$\Delta G^* = \Delta G^{*'} - KT\ell n\Gamma$$

where $KT\ell n\Gamma$ is taken as the sum of the additional free energy terms prescribed by the revised theory. The factor Γ is commonly referred to as the "gasification factor". Note that because of the form of the additional free energy terms in the expression above, the nucleation rate equation may be rewritten as

$$J = C\Gamma \exp(-\Delta G^{*'}/KT) \tag{5}$$

with the gasification factor appearing as a pre-exponential. Then, for the classical theory, $\Gamma = 1$ and $\Delta G^{*'} = \Delta G^*$.

Now, since we have removed the additional free energy terms from the exponential, we may consider the calculation of g^* and r^*. It is known that they may be related geometrically by

$$g^* v_L = \frac{4}{3}\pi (r^*)^3 \tag{6}$$

where v_L is the volume of a condensate molecule.

Also, since ΔG^* is a maximum for r^* (and g^*), the differential of equation (4) with respect to g^* may be set equal to zero. The term dr^*/dg^* which occurs in this differential may be found by differentiating equation (6).

$$r^* = \frac{2\sigma v_L}{KT\ell nS} \tag{7}$$

$$g^* = \frac{2}{3} \frac{4\pi(r^*)^2\sigma}{KT\ell nS}$$

$$\text{or} \quad g^* = \frac{32}{3} \frac{\sigma^3 v_L^2}{(KT\ell nS)^3} \tag{8}$$

Substituting the values into equation (4), and noting also that v_L is inversely proportional to ρ_L, the liquid density, it appears that the nucleation rate J as given in equation (5) will have an exponential term due to $\Delta G^{*'}$ which is proportional to

$$\frac{\sigma^3}{\rho_L^2}$$

indicating a high degree of sensitivity to the physical properties of the fluid.

The equation for the gasification factor, Γ, is quite complicated, and an approximation shown below was used to calculate values of Γ for benzene and chloroform.

$$\Gamma = \left[\frac{g^* \bar{M}_v T}{10^5}\right]^4 \frac{10^{11}}{\rho_L p} \tag{19}$$

where $\bar{M}_v$ is the molecular weight of the vapor

p is the vapor partial pressure in atmospheres

ρ_L is the liquid density in gm/cc

T is the temperature in $^{\circ}K$

Values of Γ for typical conditions for both benzene and chloroform were in the range 10^{14} to 10^{16}.

The pre-exponential factor, C, in equation (5) is essentially the concentration of single molecules times the impingement frequency of single molecules on critical-sized clusters.

The expression derived by Frenkel (1946) is shown below.

$$C = \left(\frac{p}{KT}\right)^2 v_L \left(\frac{2\sigma}{\pi \bar{m}}\right)^{1/2} \qquad (10)$$

where $\bar{m}$ is the mass of the molecule.

The equations presented above represent a considerable simplification of nucleation theory. For a more detailed treatment, the reader is referred to Frenkel (1946) for the classical theory, and to Feder, Russell, Lothe and Pound (1966) for the revised as well as the classical theory.

C. Drop Growth

The development of the equation for the growth of the condensed droplets makes use of the following assumptions:

1. The velocity distribution of the vapor molecules is Maxwellian before collision, and after reflection or evaporation.
2. The droplets are spherical.
3. Reflected molecules have come to thermal equilibrium with the droplet before leaving its surface.
4. The rate of evaporation from the droplet is equivalent to the equilibrium rate of condensation at the droplet temperature and pressure.
5. The vapor surrounding the droplets is a mixture of perfect gases.

We may assume that only a fraction of the molecules which collide with the droplet attach themselves to it. This fraction of the colliding molecules which does not reflect is given by ξ, the mass accommodation coefficient or "sticking" coefficient. The remainder, or $(1-\xi)$, are reflected.

β, the rate at which molecules strike the droplet surface, is equal to $p/(2\pi RT)^{1/2}$. If the fraction $(1-\xi)$ are reflected, then the mass flux into the droplet must be

$$\xi\beta = \xi \frac{p}{\sqrt{2\pi RT}}$$

and by the assumption 4, the mass flux evaporating from the droplet is

$$\xi\beta_D = \xi \frac{p_D}{\sqrt{2\pi RT_D}}$$

where the vapor pressure surrounding the spherical droplet of radius r is related to the flat-film saturation pressure at the droplet temperature by:

$$\ell n \frac{p_D}{(p_\infty)_D} = \frac{2\sigma}{\rho_L R T_D r}$$

The conservation of mass may be written

$$\frac{dr}{dt} = \frac{\xi}{\rho_L} (\beta - \beta_D) \tag{11}$$

The energy flux per unit area to the drop is $\beta(ZRT)$, where $Z = ([1/(\gamma-1)] + 1/2)$. The energy flux away from the droplet due to reflection is $(1-\xi)\ \beta\ (ZRT_D)$, by assumption 3. The evaporating mass flux also carries the energy $\xi\beta_D(ZRT_D)$.

The rate of change of the internal energy of the droplet is

$$\frac{4}{3}\pi r^3 \rho_L c_L \frac{dT_D}{dt} + 4\pi r^2 \frac{dr}{dt} \rho_L U_{f_D}$$

where $$U_{f_D} \simeq h_{fg} = \left(\frac{\gamma}{\gamma-1}\right) RT_D - (h_{fg})_D \tag{12}$$

c_L = specific heat of condensate

Thus, conservation of energy may be written

$$\frac{4}{3}\pi r^3 \rho_L c_L \frac{dT_D}{dt} + 4\pi r^2 \frac{dr}{dt} \rho_L U_{f_D} =$$

$$4\pi r^2 [\beta(ZRT) - (1-\xi)\ \beta\ (ZRT_D) - \xi\beta_D(ZRT_D)] \tag{13}$$

Combining with equations (11) and (12), this may be rewritten as

$$\xi(Z-\phi)\left(1 - \frac{\beta_D}{\beta}\right) - Z\left(1 - \frac{T}{T_D}\right) = 0 \tag{14}$$

where $$\phi \equiv \frac{\gamma}{\gamma-1} - \frac{h_{fg}}{RT_D}$$

To account for collisions of the vapor with the carrier gas, another term may be added to equation (14) of the form

$$-Z_c \left(\frac{\beta c}{\beta}\right) \left(1 - \frac{T}{T_D}\right) \frac{\bar{M}_v}{\bar{M}_c}$$

where subscript c refers to the carrier gas.

With these relations, T_D and dr/dt may be evaluated if an initial radius is assumed. It is now possible to find μ and $d\mu$, and hence the four unknowns ($d\mu/dx$, dP/dx, dT/dx, dM/dx) are related by four equations. A Runge-Kutta numerical integration procedure may be applied to solve these differential equations:

$$dY_1 = 8\pi JA$$

$$dY_2 = Y_1 \frac{dr}{dt} + r^* dY_1$$

$$dY_3 = Y_2 \frac{dr}{dt} + JA\,(4\pi r^{*2})$$

$$dY_4 = \frac{d\mu}{dx} = \frac{\rho_L}{\dot{m}} \left[Y_3 \frac{dr}{dt} + JA\left(\frac{4}{3}\pi r^{*3}\right)\right]$$

$$dY_5 = \frac{dP}{dx} = P\left[\left(\frac{h_{fg}}{\theta C_p' T} - \psi\right) \frac{d\mu}{dx} - \frac{1}{A}\frac{dA}{dx}\right] \left[1 - \frac{1-\mu}{\gamma M^2} - \frac{(\gamma-1)(1-\mu)}{\theta\gamma}\right]^{-1}$$

$$dY_6 = \frac{dT}{dx} = T\left[\frac{(\gamma-1)(1-\mu)}{\theta\gamma} \frac{1}{P} \frac{dP}{dx} + \frac{h_{fg}}{\theta C_p' T} \frac{d\mu}{dx}\right]$$

$$dY_7 = \frac{dM}{dx} = -M\left[\frac{1-\mu}{\gamma M^2} \frac{1}{P}\frac{dP}{dx} + \frac{1}{2}\left(\frac{1}{\gamma}\frac{d\gamma}{dx} + \frac{1}{T}\frac{dT}{dx} + \frac{1}{R}\frac{dR}{dx}\right)\right]$$

dY_1, dY_2 and dY_3 are variables which are created to make the solution easier. Details of the derivation of the last four equations are presented in Appendix C, which also explains the meaning of θ and ψ (variables introduced to reduce the complexity of the above equations).

IV. COMPARISON OF THEORY WITH EXPERIMENTAL DATA

The primary purpose of this experiment was to provide experimental data with which to compare theoretical data computed by the methods presented in the preceding section. There are two major parameters which are useful in comparing theory with data.

A. Incidence of Condensation

For a given set of inlet conditions, theory should correctly predict the point of incidence, which corresponds roughly to the point of maximum nucleation rate. The nucleation rate equation as developed in III.B is affected to a great degree by two factors: the pre-exponential gasification factor (Γ), and the free energy barrier to nucleation ($\Delta G^{*'}$).

The classical theory of nucleation predicts a Γ of 1, whereas revised theory predicts a Γ of 10^{14}-10^{15} for benzene, and 10^{15}- 10^{16} for chloroform. Thus, with a theoretical nucleation rate that is 10^{14}-10^{16} greater than that predicted by classical theory, the incidence of condensation will occur at much lower supersaturations for revised theory.

It has been shown previously that $\Delta G^{*'}$ is strongly dependent on the physical properties of the fluid. In particular, it is proportional to the cube of the surface tension. Therefore, a rise in surface tension will result in a greater barrier to nucleation, and consequently a greater supersaturation will be necessary for condensation to occur.

Because of the small size of the liquid droplets, it is not necessarily correct to assume that the surface tension (σ) of these droplets is the same as the flat-film surface tension (σ_∞). However, a problem arises in that there is disagreement over the direction toward which the correction in the flat-film values should go. Kirkwood and Buff (1949), for instance,

predict a reduction in surface tension with increasing curvature, whereas Oriani and Sundquist (1963) predict just the opposite for very small (10-100 molecules) droplets. The range of values for σ/σ_∞ may go from about 0.8 to 1.2, and as a result the correction which is made for the surface tension may either raise or lower the point of incidence, depending on which correction is adopted.

For both benzene and chloroform, the point of incidence may be predicted quite accurately by assuming a certain value of Γ. For chloroform, a Γ of 10^{16} or greater provides good agreement on incidence between theory and data, as shown by Figures 12 through 14. The data on incidence for all chloroform tests is summarized in Figure 15, which is a log-log plot of incident pressures and temperatures. Also plotted on this are the saturation pressure, and lines of predicted incidence for $\Gamma=1$ (classical theory) and $\Gamma=10^{16}$ (revised theory). Again, note that the data agree much better with revised theory than with classical theory.

For benzene, a Γ of 10^{7}-10^{8} provides good agreement between theory and data, while neither revised nor classical theory will agree with data unless some modification (to the surface tension, for instance) is made. Figures 6 through 8a demonstrate the relatively accurate prediction of incidence for $\Gamma=10^{8}$, and in Figure 9 the incidence data for all benzene tests is summarized. The lines of predicted incidence in Figure 9 for $\Gamma=1$, $\Gamma=10^{8}$ and $\Gamma=10^{15}$ also show the good agreement for 10^{8}, and the poor agreement for classical and revised theories.

However, in the case of benzene where the incidence data appears to fall about midway between revised and classical theories, it is possible to modify the surface tension data such that both theories may be made to agree with experimental incidence data. If it is assumed that the Oriani and Sundquist

correction to flat-film surface tension is correct, and the flat-film values are increased by about 10%, then the incident points now predicted by revised theory will show more agreement with data (see Figure 8c). Conversely, if the Kirkwood and Buff correction is adopted, and flat-film surface tension is reduced by about 20%, then classical theory will now correctly predict points of incidence (see Figure 8b). While this "curve-fitting" is arbitrary, it does demonstrate the effect which uncertainity concerning the surface tension can have.

B. Pressure Profile Shape

The pressure profile shape may be considered in two parts: the shape following incidence, and the total pressure rise far downstream where nearly all the vapor has condensed.

The latter is a function primarily of the amount of vapor injected, and the heat of vaporization of the fluid. It is essentially independent of the point of incidence and the profile shape farther upstream.

The shape of the pressure profile following the incidence of condensation is a function primarily of the condensation coefficient, ξ, although it is also affected to a lesser degree by the point of incidence and the amount and type of vapor injected.

Considering equation (1), incidence of condensation close to the throat (M=1) will tend to accentuate the pressure rise closely following incidence, which will often give a "hump" to the pressure profile rather than a "ramp". This may be seen in Figure 11, for chloroform condensation, where a rise in inlet temperature lowers the point of incidence, smoothing out the hump.

The effect of the amount and type of injected vapor on the profile shape following incidence is similar to the effect these have on the downstream pressure rise. The more latent heat that is released, the greater the rise

in pressure.

The condensation coefficient (ξ) represents the fraction of molecules which collide with a droplet which are not reflected. The lower the value of ξ, the more the growth of the condensate droplets is retarded. A low ξ (less than about 0.1) will tend to smooth out the profile, and the pressure rise will not reach its final height until far downstream. The condensation coefficient should not be too important a factor for either benzene or chloroform. Hirth and Pound (1963) predict ξ=0.9 for benzene, and ξ=0.5 for chloroform.

The comparison of theory with data in Figures 6 through 8 (for benzene) and 12 through 14 (for chloroform) show that agreement on the pressure profile shape is only fair, although it is certainly much better for chloroform than for benzene. In particular, the profile shape following incidence for the chloroform data is quite good, and deviation between theory and data which occurs farther downstream is minor. The benzene profiles do not correspond either on the shape following incidence or on the downstream shape.

The fact that the theoretical downstream profile shape for benzene (and chloroform, to a lesser extent) deviates from the experimental shape would seem to mean that the amount of vapor injected was incorrectly measured, or that a mistake was made in deriving the theoretical equations, or the data for heat of vaporization was incorrect. All three possibilities have been checked, with no error being found.

V. SUMMARY AND CONCLUSIONS

The comparison of theory and data for benzene condensation offers support for neither the classical nor the revised nucleation theories. If an arbitrary pre-exponential factor of 10^7-10^8 is put into the nucleation rate equation, the point of incidence can be accurately predicted for a wide range of initial conditions. The summary of incidence data in Figure 9 shows the good agreement of theory with data for a pre-exponential factor of 10^8, and also shows the absence of any substantial scatter in the experimental points of incidence. By making an arbitrary reduction in surface tension of about 20%, it is possible to get good agreement on incidence points between data and classical theory (Γ=1). By a similarly arbitrary increase in surface tension of 10%, it is also possible to get good agreement between revised theory ($\Gamma=10^{15}$) and experimental data.

The downstream pressure profile shape for benzene does not agree well with theoretical predictions, either in the shape immediately following incidence or in the shape far downstream. The reason for the disagreement is not clear, but since the profile shape is not closely related to the point of incidence, conclusions on nucleation theory should not be affected.

Revised nucleation theory ($\Gamma=10^{16}$) shows good agreement with experimental chloroform data. The point of incidence of condensation may be predicted accurately by a pre-exponential factor of 10^{16} or greater, as shown in Figures 12 through 14 and summarized in Figure 15. The predicted pressure profile shape following incidence and farther downstream both correspond closely to data. Classical theory will predict correct points of incidence only for a substantial (30% or more) decrease in surface tension.

For both benzene and chloroform condensation, there was no apparent change in either point of incidence or pressure profile shape when the moisture content of the carrier air was reduced by the use of the cold trap,

as shown in the incidence plots (Figures 9 and 15).

As explained in Appendix D, there was apparently a slight decrease in boundary layer thickness when benzene and chloroform were mixed with the carrier air, but the effect was small and could be taken into account when experimental data were plotted.

In conclusion, it appears that the condensation behavior of chloroform may be predicted with good precision if the revised theroy of nucleation is adopted. Benzene condensation data appears to agree with neither classical nor revised theory, and instead falls about midway between the predicted behavior of these two theories.

The prediciton of the pressure profile shape following incidence does not in all cases agree with experimental data. Although this should have little affect on the conclusions made concerning nucleation theory, it does deserve further investigation. Since this represents the first time that relatively heavy molecules have been tested in the Gas Turbine Laboratory, it would seem desirable that more large molecular weight substances be tested.

Despite the fact that chloroform condensation showed good agreement with revised nucleation theory, it doesn't appear that any general conclusions concerning the applicability of either theory may yet be made. Based on current data, water vapor and carbon dioxide agree well with classical theory, ammonia and chloroform agree well with revised theory, and benzene agrees with neither theory. This would seem to lend support to the conclusion of Jaeger (1966) that neither theory is applicable in its present form, since both theories assign bulk properties to very small droplets. In the case of surface tension in particular, this assumption does not seem to be valid.

TABLE I SUMMARY OF BENZENE EXPERIMENTS AND RESULTS

	INITIAL CONDITIONS			CARRIER AIR		CONDITIONS AT INCIDENCE			
Test No.	ω_o	P_o (Atm)	T_o (°K)	Dew Point (°F)	$(\frac{P}{P_o})_i$	p_i (Atm)	p_i (mm Hg)	T_i (°K)	S_i
1	.063	3.99	315	-60	.240	.0234	17.8	214	60
2	.080	4.00	318	-60	.245	.0307	23.3	218	52
3	.087	4.03	320	-60	.240	.0329	25.0	219	50
4	.096	4.02	321	-60	.250	.0384	29.2	223	40
5	.104	4.02	322	-60	.260	.0434	33.0	226	34
6	.080	4.02	322	-60	.220	.0278	21.1	215	65
7	.087	4.02	332	-60	.220	.0304	23.1	222	35
8	.079	4.02	332	-60	.220	.0271	20.6	221	34
9	.116	4.03	331	-60	.225	.0421	32.0	224	40
10	.074	3.97	322	-60	.235	.0268	20.4	218	45
11	.094	4.01	322	-60	.245	.0367	27.9	222	42
12	.096	4.01	332	-60	.235	.0357	27.1	226	28
13	.109	4.01	332	-60	.250	.0432	32.8	231	23
14	.092	4.01	322	-60	.245	.0355	27.0	222	41
15	.094	4.01	332	-60	.230	.0342	26.0	225	30
16	.087	4.01	332	-60	.200	.0275	20.9	217	53
17	.086	3.77	332	-60	.225	.0286	21.7	223	30
18	.034	3.98	312	-60	.175	.0091	6.9	192	294
19	.037	3.74	332	-150	.155	.0082	6.3	198	126
20	.038	3.95	309	-60	.175	.0099	7.6	191	370
21	.044	3.94	311	-60	.180	.0119	9.1	194	293
22	.049	3.94	312	-60	.205	.0154	11.7	202	148

TABLE I SUMMARY OF BENZENE EXPERIMENTS AND RESULTS (CONT.)

	INITIAL CONDITIONS			CARRIER AIR	CONDITIONS AT INCIDENCE				
Test No.	ω_o	P_o (Atm)	T_o	Dew Point (°F)	$(\frac{P}{P_o})_i$	p_i (Atm)	p_i (mm Hg)	T_i (°K)	S_i
23	.053	3.94	312	-60	.225	.0182	13.8	208	86
24	.032	4.02	305	-60	.195	.0096	7.3	193	270
25	.036	4.02	306	-60	.195	.0108	8.2	195	237
26	.040	4.03	307	-60	.205	.0126	9.6	198	192
27	.043	4.03	309	-60	.215	.0139	10.6	202	134
28	.046	4.04	310	-60	.220	.0155	11.8	204	118
29	.049	4.04	309	-60	.220	.0168	12.8	204	128
30	.057	3.71	311	-150	.225	.0184	14.0	207	100
31	.054	3.71	311	-150	.220	.0170	12.9	206	102
32	.044	3.74	305	-150	.210	.0131	9.9	198	198
33	.041	3.75	310	-150	.175	.0103	7.8	191	381
34	.037	3.76	307	-150	.190	.0101	7.7	194	248
35	.043	3.77	309	-150	.210	.0130	9.9	201	143
36	.046	3.77	308	-150	.220	.0147	11.2	203	129
37	.051	3.77	309	-150	.225	.0165	12.5	205	114
38	.054	3.77	309	-150	.235	.0184	14.0	208	87
39	.039	3.65	307	-150	.190	.0103	7.8	194	251
40	.044	3.65	307	-150	.195	.0121	9.2	196	236
41	.049	3.65	307	-150	.200	.0139	10.6	198	212
42	.054	3.65	308	-150	.215	.0163	12.4	202	157
43	.058	3.64	309	-150	.225	.0184	14.0	205	127

TABLE II SUMMARY OF CHLOROFORM EXPERIMENTS AND RESULTS

	INITIAL CONDITIONS			CARRIER AIR	CONDITIONS AT INCIDENCE				
Test No.	ω_o	P_o (Atm)	T_o (°K)	Dew Point (°F)	$(\frac{P}{P_o})_i$	p_i (Atm)	p_i (mm Hg)	T_i (°K)	S_i
44	.142	3.69	311	-60	.280	.0433	32.9	223	16
45	.168	3.70	311	-150	.290	.0503	38.2	226	14
46	.176	3.71	332	-60	.230	.0420	31.9	227	11
47	.190	3.72	341	-60	.210	.0421	32.0	229	10
48	.043	3.68	303	-60	.210	.0084	6.4	196	38
49	.047	3.68	305	-60	.215	.0092	7.0	199	30
50	.050	3.69	310	-60	.210	.0097	7.4	201	26
51	.054	3.69	311	-60	.210	.0105	8.0	202	25
52	.058	3.70	312	-60	.210	.0116	8.8	203	26
53	.062	3.70	314	-60	.210	.0124	9.4	204	25
54	.066	3.70	315	-60	.215	.0134	10.2	206	22
55	.069	3.70	315	-150	.220	.0143	10.9	208	20
56	.073	3.70	316	-150	.225	.0155	11.8	210	18
57	.075	3.70	316	-150	.230	.0165	12.5	212	15
58	.132	3.71	332	-60	.210	.0278	21.1	219	14
59	.144	3.71	332	-60	.215	.0313	23.8	222	12
60	.155	3.72	333	-60	.220	.0347	26.4	224	12
61	.165	3.74	333	-60	.220	.0374	28.4	225	12
62	.175	3.73	331	-60	.225	.0412	31.3	225	13
63	.185	3.74	331	-60	.225	.0441	33.5	226	13
64	.196	3.75	331	-60	.225	.0471	35.8	227	13
65	.205	3.75	331	-60	.225	.0499	37.9	227	13
66	.165	3.73	312	-150	.265	.0468	33.6	223	15
67	.200	3.73	315	-60	.245	.0569	36.2	225	16

REFERENCES

Becker, R. and Doring, W. - Ann. der Physik - Vol. 24, p. 719, 1935.

Binnie, A. M. and Green, J. R. - Proc. Roy. Soc. - Vol. 181A, p. 134, 1942.

Binnie, A. M. and Woods, M. W. - Proc. Inst. of Mech. Eng. - Vol. 138, p. 229, 1938.

Duff, K. - "Non-Equilibrium Condensation of Carbon Dioxide in Supersonic Nozzles" - Gas Turbine Laboratory Report #84 - M.I.T., 1966.

Feder, J., Russell, K. C., Lothe, J. and Pound, G. M. - Adv. in Physics - Vol.15, p. 1, Jan. 1966.

Frenkel, J. - Kinetic Theory of Liquids - Oxford University Press, 1946.

Gottschall, A. J., and Korvezee, A. E. - Recueil des Travaux Chimiques des Pays - Vol. 72, p. 473, 1953.

Handbook of Chemistry and Physics - 43rd Edition - The Chemical Rubber Publishing Co., Cleveland, Ohio, 1961.

Hill, P. G. - "Homogeneous Nucleation of Supersaturated Water Vapor in Nozzles" - Gas Turbine Laboratory Report #78 - M.I.T., 1965.

Hirth, J. P. and Pound, G. M. - Progress in Materials Science, Vol. 11 - "Condensation and Evaporation" - Macmillan, New York, 1963.

International Critical Tables - National Research Council - McGraw-Hill, New York, 1928.

Jaeger, H. L. - "Condensation of Supersaturated Ammonia and Water Vapor in Supersonic Nozzles" - Gas Turbine Laboratory Report #86 - M.I.T., 1966.

Keenan, J. H. and Kaye, J. - Gas Tables - John Wiley and Sons, Inc., 1945.

Kirkwood, J. and Buff, F. - Jour. of Chem. Physics - Vol. 17, p. 338, 1949.

Kremmer, M. and Okurounmu, O. - "Condensation of Ammonia Vapor During Rapid Expansion" - Gas Turbine Laboratory Report #79 - M.I.T., 1965.

Kuhrt. F. - Z. Physik - Vol. 131, p. 185, 1952.

Kuss, E. - Z. fur angewandte Physik - Vol. 7, p. 372, 1955.

Lothe, J. and Pound, G. M. - Jour. of Chem. Physics - Vol. 36, p. 2080, 1962.

Metzger, E. - Jour. de Physique et le Radium - Vol. 7, p. 303, 1946.

Oriani, R. A. and Sundquist, B. E. - Jour. of Chem. Physics - Vol. 38, p. 2082, 1963.

Oswatitsh, K. - Z. fur angewandte Math. und Mechanik - Vol. 22, p. 14, 1942.

Powell, C. F. - Proc. Roy. Soc. (London) - Vol. 119A, p. 55, 1928.

Rettaliata, J. T. - Trans. ASME - Vol. 58, p. 599, 1936.

Rodebush, W. H. - Chemical Reviews - Vol. 44, p. 269, 1949.

Rodebush, W. H. - Industrial Eng. Chemistry - Vol. 44, p. 1289, 1952.

Scharrer, L. - Ann. der Phys. Leipzig, Vol. 35, p. 619, 1939.

Shapiro, A. H. - The Dynamics and Thermodynamics of Compressible Fluid Flow - The Roland Press Co., New York, 1953.

Stever, H. G. and Rathbun, K. C. - "Theoretical and Experimental Investigation of Condensation of Air in the Hypersonic Wind Tunnel" - N.A.C.A. Technical Note 2559, Nov. 1951.

Stever, H. G. - "Condensation in High Speed Flows", High Speed Aerodynamics and Jet Propulsion - Vol. III, p. 526, Princeton Univ. Press, 1958.

Stodola, A. - Steam and Gas Turbines - McGraw-Hill Book Co., Inc., p. 117, p. 1034, 1927.

Timmermans, J. - Physico-Chemical Constants of Pure Organic Compounds - Elsevier Publishing Co., New York, 1956, 1965, 2 volumes.

Volmer, M. - Kinetik der Phasenbildung - Steinkopff, Dresden u. Leipzig, 1939.

Volmer, M. and Flood, H. - Z. fur physik. Chemie - Vol. 170A, p. 273, 1934.

Wegener, P. P. - "Condensation Phenomena in Nozzles" - A.I.A.A. Preprint #63, 1963.

Wegener, P. P. and Pouring, A. A. - The Physics of Fluids - Vol. 7, p. 352, 1964.

Wilson, C. T. R. - Phil. Trans. Royal Soc. - Vol. 192A, p. 403, 1899; also - Phil. Trans. Royal Soc. - Vol. 193A, p. 289, 1900.

Yellot, J. I. - Trans. ASME - Vol. 56, p. 411, 1934.

APPENDIX A METERING OF THE INJECTED VAPOR

The mass flow rate of the injected vapors was measured by the pressure drop across a calibrated orifice. The liquid benzene and chloroform were stored in a pressurized stainless steel tank with a capacity of about two gallons. The tank was pressurized by undried air directly from the compressor, and by means of a regulator on the air inlet line the tank pressure could be varied from 0 to about 90 psig (the maximum pressure available from the surge tank). The pressure on the downstream side of the orifice was fixed by the stagnation pressure at the nozzle inlet and was usually on the order of 40 to 45 psig.

The static pressure on either side of the orifice was measured by means of taps connected to a strain-gauge-type pressure transducer ("Dynisco" No. APT 25R SP-LC) with a range of 0 to 100 psia. As shown in Fig. A-1, the response (in millivolts) of the transducer to changes in pressure is linear. Because the pressure difference across the orifice was measured rather than the absolute pressures, it was necessary only to check the slope of the response vs. applied pressure curve. This was accomplished by noting the change in response from a known pressure difference, such as the difference between stagnation pressure at nozzle inlet and atmospheric pressure (the former measured with a mercury-filled U-tube, and the latter by a barometer). For this purpose, connections to the transducer from the stagnation pressure tap and the atmosphere were provided in addition to the taps upstream and downstream of the orifice (see Fig. A-2).

Two orifices were used to provide a wide range of flow rates. They consisted of discs of .005" stainless sheet pierced by holes of about .007"

diameter for one, and .018" diameter for the other. They were calibrated for both benzene and chloroform by discharging at atmospheric pressure into plastic bags, which were then weighed. The pressure difference across the orifice was measured with the pressure transducer. During both calibration and experimental runs, correction was made for the height of the liquid column when the transducer was connected to the tap upstream of the orifice. Calibration curves (mass flow rate vs. pressure difference) for both orifices are shown in Fig. A-3 and Fig. A-4.

FIGURE A-1 CALIBRATION CURVE FOR PRESSURE TRANSDUCER

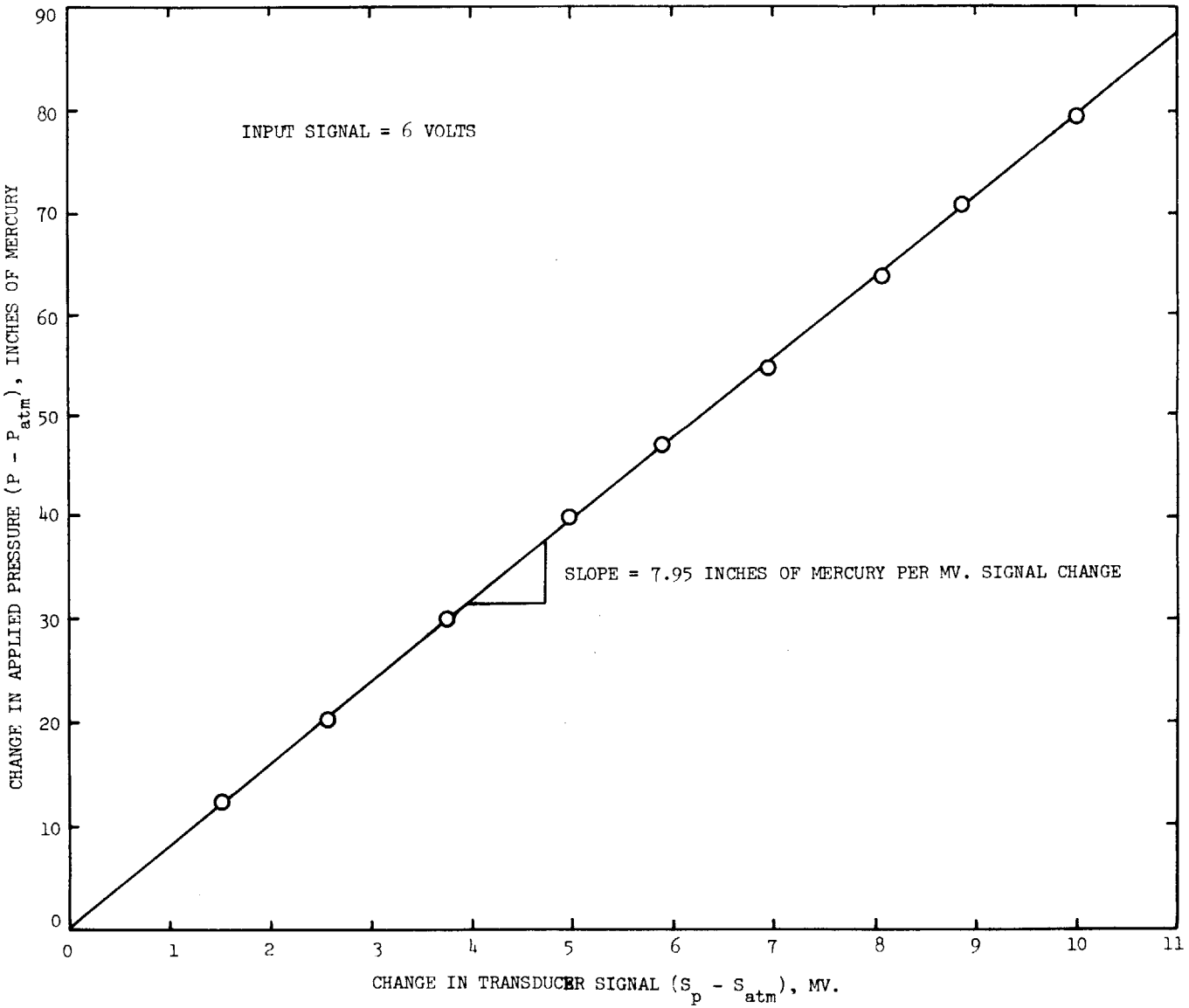

FIGURE A-2 SCHEMATIC DIAGRAM OF PRESSURE TRANSDUCER CONNECTIONS

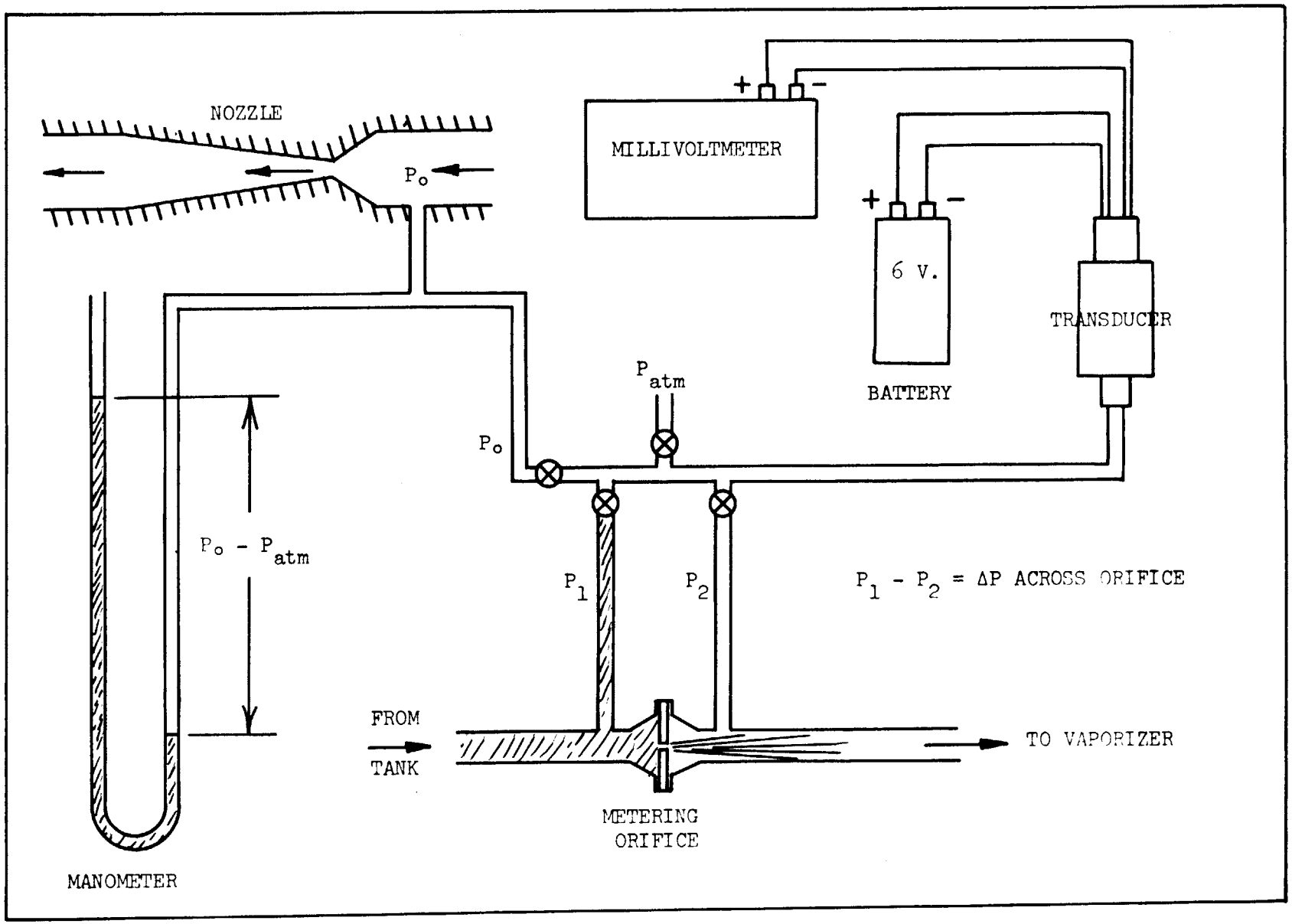

FIGURE A-3 CALIBRATION CURVE FOR .007" METERING ORIFICE

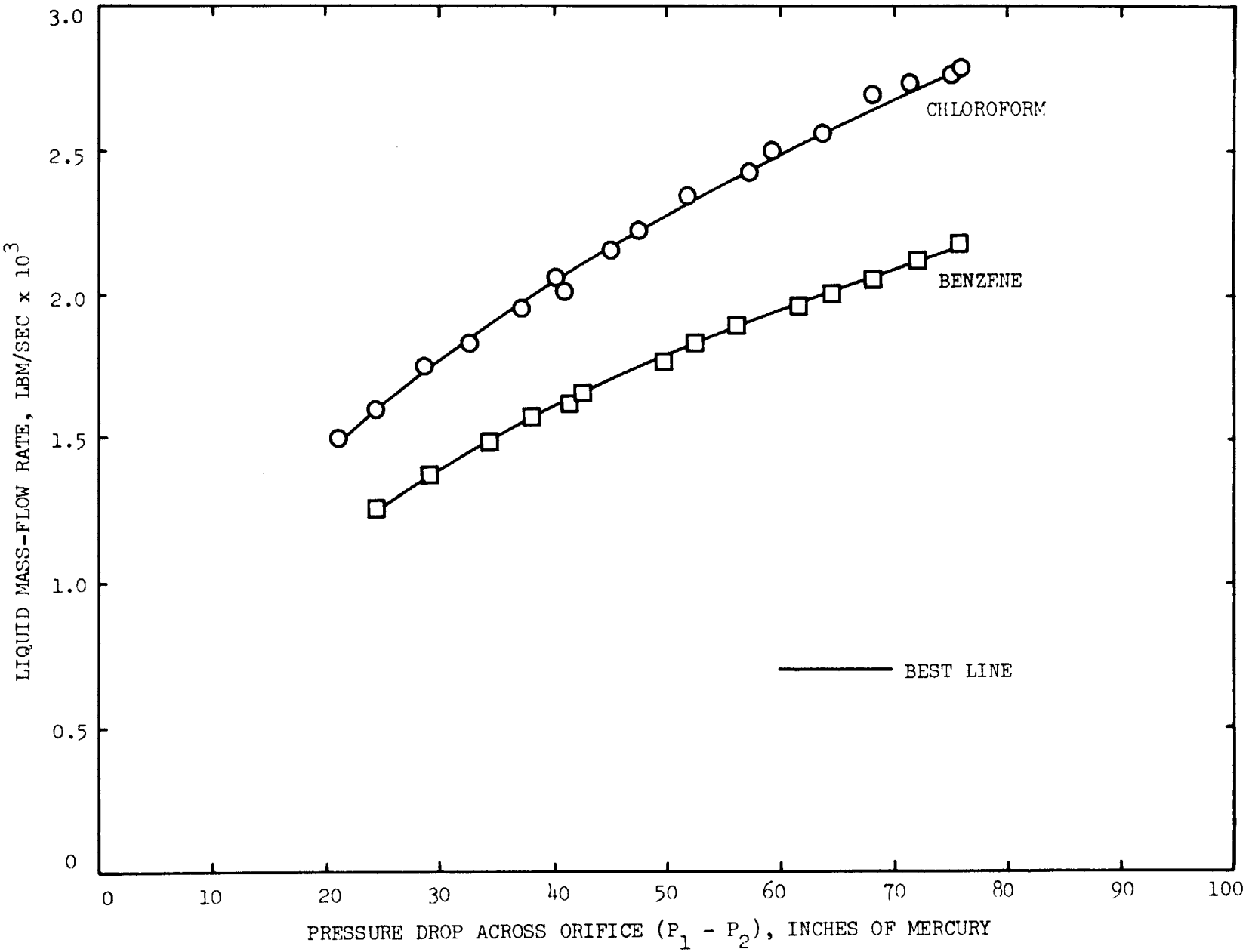

FIGURE A-4 CALIBRATION CURVE FOR .018" METERING ORIFICE

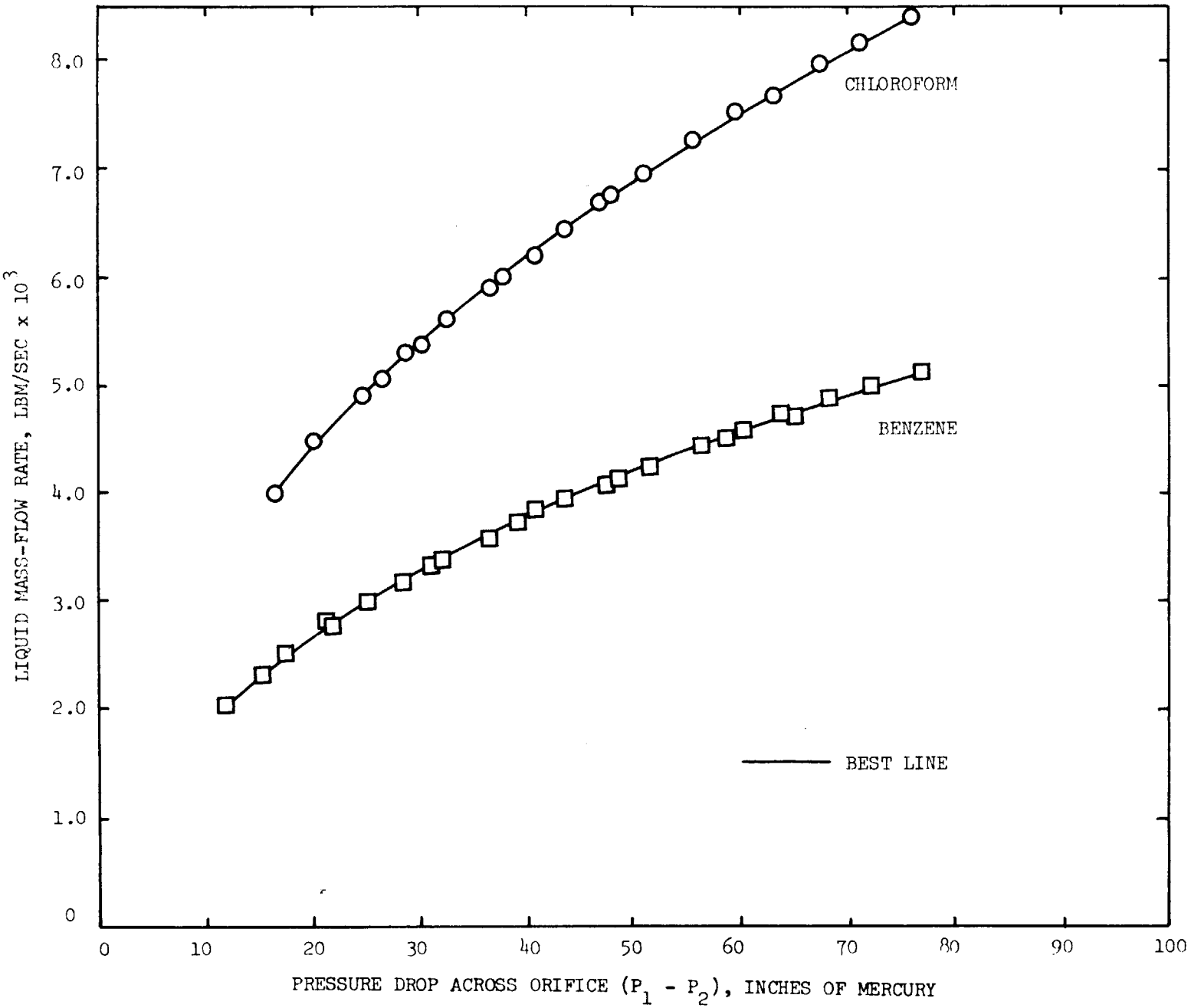

APPENDIX B CALCULATION OF ω_o AND y_o

In determining the theoretical pressure distribution in the nozzle, it is necessary to know ω_o, the mass fraction of vapor at nozzle inlet for the vapor-carrier air mixture, and y_o, the corresponding mole fraction. The stagnation temperature and pressure (T_o and P_o) are measured for each experimental run, and $\dot{m}_v$ (the mass flow rate of vapor) may be found from the pressure drop across the metering orifice and the calibration curve for that orifice (see Appendix A). In addition, the following quantities may be assumed known:

A^*

M_v

γ_v

M_c

γ_c

The mass fraction of the injected vapor is given by:

$$\omega_o = \frac{\dot{m} \text{ vapor}}{\dot{m} \text{ mixture}} \tag{B.1}$$

where $\dot{m}_{mixture} = \dot{m}_v + \dot{m}_c$

The mole fraction may then be found since

$$y_o = \omega_o \frac{\bar{M}_m}{\bar{M}_v} \tag{B.2}$$

If we assume choked flow for the nozzle, the mass flow rate of the mixture may be found from the perfect-gas, isentropic-flow relation

$$\dot{m} = \frac{A^* P_o}{\sqrt{T_o}} \sqrt{\frac{\gamma}{\bar{R}/\bar{M}} \left(\frac{2}{\gamma+1} \right)^{\frac{\gamma+1}{\gamma-1}}} \tag{B.3}$$

where the γ and M are those of the mixture, and $\bar{R}$ is the universal gas constant.

The molecular weight $\bar{M}_m$ of the mixture is given by

$$\bar{M}_m = y_o \bar{M}_v + (1-y_o)\bar{M}_c \tag{B.4}$$

and γ_m is given by:

$$\gamma_m = \frac{y_o \left(\frac{\gamma_v}{\gamma_v - 1}\right) + (1-y_o)\left(\frac{\gamma_c}{\gamma_c - 1}\right)}{y_o \left(\frac{1}{\gamma_v - 1}\right) + (1-y_o)\left(\frac{1}{\gamma_c - 1}\right)} \tag{B.5}$$

The procedure followed was to assume values of γ_m and $\bar{M}_m$ and use equation (B.3) to find $\dot{m}_m$. Using this in (B.1), a value of ω_o can be found, from which y_o can be found using (B.2). From (B.4) and (B.5) new values of γ_m and $\bar{M}_m$ can be computed, and if these do not agree well with the assumed values, $\dot{m}_m$ can be recomputed and the entire procedure repeated. In general, by judicious choice of the assumed values of γ_m and $\bar{M}_m$ it was usually possible to find ω_o and y_o in a single iteration.

In equation (B.3) the value of A^* is assumed to be .0292 square inches. This represents the geometrical area of the throat rather than the effective flow area, but Duff (1966) has shown that the boundary layer at the throat of this nozzle is thin enough to be neglected in the mass-flow calculation.

APPENDIX C DERIVATION OF GAS DYNAMIC RELATIONS

The equations for dP/P, dT/T, du/u and dM/M are derived from four relations: continuity, conservation of energy, conservation of momentum and the equation of state for a perfect gas.

1. Conservation of Mass (Continuity)

$$m = \frac{\rho A \mu}{1-\mu} = \text{constant} \tag{C.1}$$

or $$\frac{d\rho}{\rho} + \frac{dA}{A} + \frac{d\mu}{\mu} + \frac{d\mu}{1-\mu} = 0 \tag{C.2}$$

where $\dot{m}$ is the total mass flow rate (carrier + vapor + liquid)

ρ is the density of gas phase

A is the effective flow area

u is the stream velocity

μ is the fraction of total mass flow that is liquid

2. Conservation of Energy

$$C_p dT + u du = h_{fg}\, d\mu$$

or $$\frac{dT}{T} + \frac{u^2}{C_p T}\,\frac{du}{u} = \frac{h_{fg}}{C_p T}\, d\mu \tag{C.3}$$

where

C_p is the specific heat at constant pressure of the total mass flow

T is the absolute temperature

h_{fg} is the heat of vaporization of the test liquid

The value of C_p at any instant may be given by

$$C_p = (1-\omega_o)C_{p_c} + (\omega_o-\mu)C_{p_v} + \mu C_{PL} \tag{C.4}$$

where ω_o is the initial fraction of the total mass flow that is vapor, and subscripts c, v, and L refer to the properties of the carrier air, vapor

and liquid, respectively. Since C_p', the specific heat of the carrier + vapor, is equal to $R\gamma/(\gamma-1)$, equation (C.4) may be rewritten

$$C_p = (1-\mu)C_p' + \mu C_{P_L}$$

$$\text{or} \quad C_p = C_p'\left[(1-\mu) + \left(\frac{\gamma-1}{\gamma}\right)\left(\frac{\mu C_{P_L} \bar{M}}{\bar{R}}\right)\right] \tag{C.5}$$

where

γ is the specific heat ratio, C_p/C_v, of the gas mixture, as calculated in equation (C.21)

$\bar{R}$ is the universal gas constant

$\bar{M}$ is the molecular weight of the gas mixture, as c alculated in equation (C.19)

The term in brackets in equation (C.5) may be referred to as θ, in which case $C_p=\theta C_p'$. With this substitution, (C.3) may be rewritten

$$\frac{dT}{T} + \frac{u^2}{\theta C_p' T}\frac{du}{u} = \frac{h_{fg}}{\theta C_p' T} d\mu \tag{C.6}$$

3. Conservation of Momentum

$$-AdP = \dot{m}du \tag{C.7}$$

or from (C.1)
$$-\frac{dP}{P} = \frac{\rho u^2}{(1-\mu)P}\frac{du}{u} \tag{C.8}$$

4. Equation of State for a Perfect Gas

$$P = \rho RT \tag{C.9}$$

or
$$\frac{dP}{P} = \frac{d\rho}{\rho} + \frac{dR}{R} + \frac{dT}{T} \tag{C.10}$$

As a convenience, the definition of Mach number is introduced, so that the velocity u may be eliminated. It is possible to define M in terms of the gas phase properties:

$$M \equiv u/(\gamma RT)^{1/2} \tag{C.11}$$

where γ refers to the specific heat ratio of the gas mixture only. The

specific heat of the gas mixture is related to γ by

$$\frac{C_p'}{R} = \frac{\gamma}{\gamma-1} \tag{C.12}$$

Combining (C.9) and (C.11) with (C.8),

$$\frac{du}{u} = -\frac{1-\mu}{\gamma M^2}\frac{dP}{P} \tag{C.13}$$

and combining (C.11) and (C.12) with (C.6),

$$\frac{dT}{T} + \frac{(\gamma-1)M^2}{\theta}\frac{du}{u} - \frac{h_{fg}}{\theta C_p'T}d\mu = 0 \tag{C.14}$$

Substituting (C.13) in (C.14),

$$\frac{dT}{T} = \frac{(\gamma-1)(1-\mu)}{\theta\gamma}\frac{dP}{P} + \frac{h_{fg}}{\theta C_p'T}d\mu \tag{C.15}$$

and combining (C.10), (C.13) and (C.15) with (C.2),

$$\frac{dP}{P}\left[1-\frac{1-\mu}{\gamma M^2}-\frac{(\gamma-1)(1-\mu)}{\theta\gamma}\right] + \frac{dA}{A} - \frac{dR}{R} + \left[\frac{1}{1-\mu} - \frac{h_{fg}}{\theta C_p'T}\right]d\mu = 0 \tag{C.16}$$

It is shown later, in (C.20), that dR/R may be given by

$$-\frac{dR}{R} = \left[\psi - \frac{1}{1-\mu}\right]d\mu$$

where

$$\psi = \left[(1-\omega_o)\frac{\bar{M}_v}{\bar{M}_c} + \omega_o - \mu\right]^{-1}$$

Thus the final form of (C.16) is

$$\frac{dP}{P} = \left[\left(\frac{h_{fg}}{\theta C_p'T} - \psi\right)d\mu - \frac{dA}{A}\right]\left[1 - \frac{1-\mu}{\gamma M^2} - \frac{(\gamma-1)(1-\mu)}{\theta\gamma}\right]^{-1} \tag{C.17}$$

The differential of (C.11) is

$$\frac{dM}{M} = \frac{du}{u} - \frac{1}{2}\frac{d\gamma}{\gamma} - \frac{1}{2}\frac{dR}{R} - \frac{1}{2}\frac{dT}{T}$$

or

$$\frac{dM}{M} = -\frac{1-\mu}{\gamma M^2}\frac{dP}{P} - \frac{1}{2}\left[\frac{d\gamma}{\gamma} + \frac{dR}{R} + \frac{dT}{T}\right] \tag{C.18}$$

where $d\gamma/\gamma$, dT/T and dR/R are given by equations (C.23), (C.15) and (C.20), respectively. The derivations of $d\gamma/\gamma$ and dR/R follow.

R, the gas constant for the mixture, is equal to $\bar{R}/\bar{M}$. Therefore, $dR/R = -d\bar{M}/\bar{M}$, where $\bar{M}$ is the molecular weight of the gas mixture.

$$\bar{M} = \frac{1-\mu}{(\frac{1-\omega_o}{\bar{M}_c}) + (\frac{\omega_o-\mu}{\bar{M}_v})} \tag{C.19}$$

$$-\frac{dR}{R} = \frac{d\bar{M}}{\bar{M}} = \left[\frac{1}{(1-\omega_o)\frac{\bar{M}_v}{\bar{M}_c} + (\omega_o-\mu)} - \frac{1}{1-\mu}\right]d\mu \tag{C.20}$$

$$\gamma = \frac{(\frac{\omega_o-\mu}{\bar{M}_v})(\frac{\gamma_v}{\gamma_v-1}) + (\frac{1-\omega_o}{\bar{M}_c})(\frac{\gamma_c}{\gamma_c-1})}{(\frac{\omega_o-\mu}{\bar{M}_v})(\frac{1}{\gamma_v-1}) + (\frac{1-\omega_o}{\bar{M}_c})(\frac{1}{\gamma_c-1})} \tag{C.21}$$

This may be rearranged as

$$\gamma = \frac{[(1-\omega_o) + (\omega_o-\mu)\,G_A]\,\gamma_c}{(1-\omega_o) + (\omega_o-\mu)\,G_B} \tag{C.22}$$

where

$$G_A \equiv (\frac{\gamma_c-1}{\gamma_c})(\frac{\gamma_v}{\gamma_v-1})\,\frac{\bar{M}_c}{\bar{M}_v}$$

$$G_B \equiv (\frac{\gamma_c-1}{\gamma_v-1})\,\frac{\bar{M}_c}{\bar{M}_v}$$

so

$$\frac{d\gamma}{\gamma} = \left[\frac{G_B}{(1-\omega_o) + (\omega_o-\mu)G_B} - \frac{G_A}{(1-\omega_o) + (\omega_o-\mu)G_A}\right]d\mu \tag{C.23}$$

Thus, the differential equations for dP/P, dT/T and dM/M may be found by (C.16), (C.15) and (C.18), respectively.

APPENDIX D EFFECT OF PRESSURE, MOISTURE AND INJECTED VAPOR ON EFFECTIVE NOZZLE FLOW AREA

Because of variations in the dry-air data on certain occasions (see Appendix F), an investigation was carried out to determine the effects of carrier air moisture and inlet pressure on the boundary layer thickness. The results of seven tests are listed in Table D. Tests A, B, D, and F were run with air directly from the dehumidifier at a dew point of -60°F. In tests C, E, and G the air was further dried by the cold trap, which reduced the dew point to -150°F. The inlet pressures for tests C, E, and G were set to match the inlet pressures of tests B, D, and F. No cold trap test could be made to correspond to test A, because the high pressure on this test was achieved by bypassing the cold trap.

The data presented shows that there is a detectable difference in pressure ratio (and hence of the effective flow area) only for substantial decreases in inlet pressure. Also, there appears to be no effect from moisture. Since all experimental runs were made with inlet pressures varying from 3.60 to 4.05 atmospheres, and with dew points of -60°F. to -150°F., it appears that carrier air moisture and changes in inlet pressure should not have had any measurable effect on the effective flow area.

There was, however, a small difference in the effective flow area due to the mixing of benzene or chloroform vapor with the air. The viscosities of both vapors are considerably less than the viscosity of air, so the addition of small quantities of benzene or chloroform will reduce the viscosity of the mixture, decreasing slightly the boundary layer thickness (which will increase the effective flow area).

This change in the flow area was measured in a crude fashion by comparing an experimental profile in the region prior to incidence with the

appropriate non-condensing isentrope. For a given pressure ratio (P/P_o), the experimental effective flow area was, in general, greater than that predicted by the theoretical isentrope, the difference being due to the change in boundary layer thickness.

Figures D-1 and D-2 show the measured area ratio (A/A^*) plotted versus the predicted area ratio for benzene and chloroform, respectively. The results indicate a slight increase in the effective area. The maximum difference in the effective area ratio, which occurs just prior to incidence, is about .005 for 8 to 10% benzene vapor, .002 for 3 to 4% benzene, and .004 for 14 to 18% chloroform. The curves in Figures D-1 and D-2 represent best lines through a group of points which exhibited considerable scatter. In some tests it appeared that the flow area had decreased, while others showed increases on the order of .007 to .010. This scatter is a reflection on the method of finding the change in the flow area. There are better methods for finding the boundary layer thickness, but this particular method was adequate for discovering the existence of a change in flow area, and for arriving at an estimate of the magnitude of the change. Corrections to data points on experimental pressure profiles could be made to account for this change, but in general the corrections were not large enough to make any observable difference in the profile.

TABLE D: PRESSURE AND MOISTURE EFFECTS ON DRY AIR DATA

Test No.	A	B	C	D	E	F	G
P_o (atm.) =	3.94	3.66	3.68	3.34	3.33	2.75	2.75
T_o (°F) =	85	85	84	85	84	84	84
Dew Point (°F) =	-60	-60	-150	-60	-150	-60	-150
X, in.	P/P_o	P/P_o	P/P_o	P/P_o	P/P_o	P/P_o	P/P_o
0.2	.376	.375	.375	.375	.375	.375	.375
0.3	.322	.321	.322	.321	.321	.320	.320
0.4	.280	.281	.280	.280	.279	.278	.277
0.5	.252	.252	.253	.252	.251	.250	.250
0.6	.230	.230	.230	.229	.229	.227	.228
0.7	.208	.208	.207	.207	.207	.206	.206
0.8	.191	.191	.191	.190	.190	.190	.190
0.9	.176	.176	.176	.175	.175	.173	.174
1.0	.163	.163	.163	.163	.163	.162	.161
1.1	.153	.153	.153	.152	.152	.151	.151
1.2	.144	.144	.144	.143	.143	.142	.141
1.3	.136	.136	.136	.134	.134	.132	.133
1.4	.127	.126	.127	.125	.126	.123	.124
1.5	.117	.117	.117	.116	.117	.116	.116
1.6	.114	.113	.113	.112	.112	.111	.111
1.7	.109	.108	.109	.109	.109	.108	.107
1.8	.102	.102	.102	.102	.102	.101	.102
1.9	.098	.097	.098	.097	.098	.096	.097
2.0	.094	.093	.093	.093	.093	.093	.093

FIGURE D-1 EFFECT OF BENZENE ON BOUNDARY LAYER THICKNESS

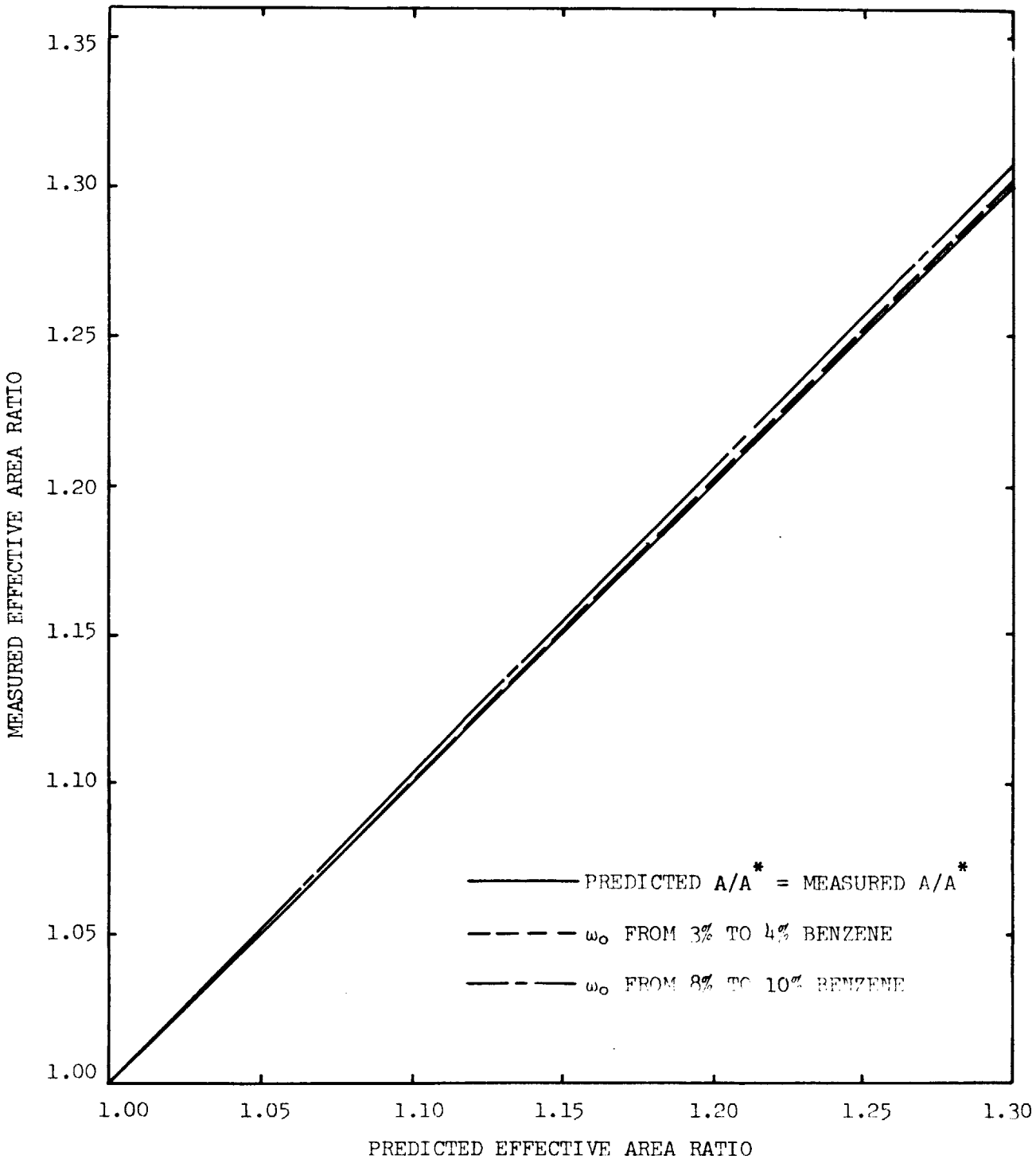

FIGURE D-2 EFFECT OF CHLOROFORM ON BOUNDARY LAYER THICKNESS

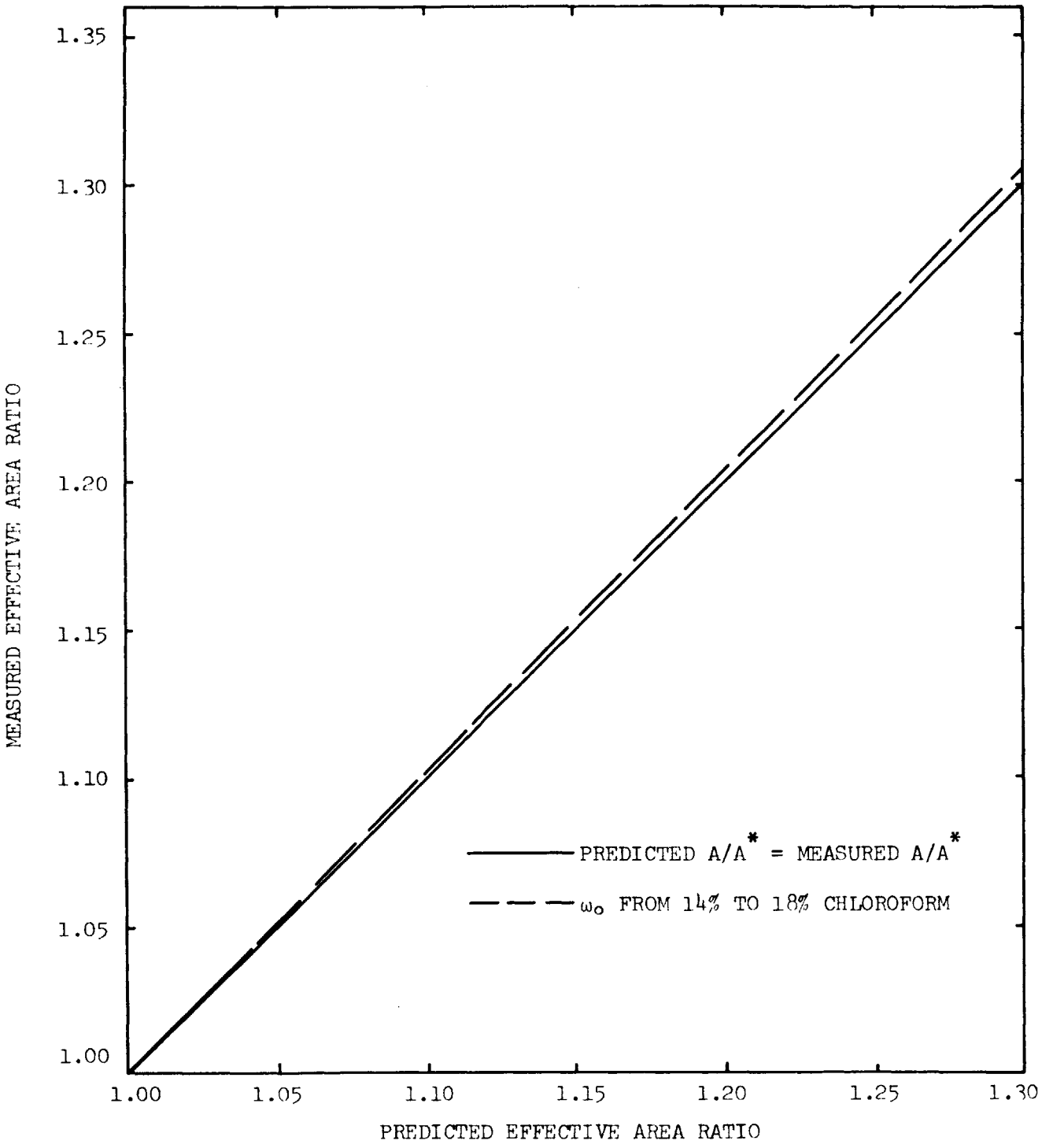

APPENDIX E CALCULATION OF THE PHYSICAL AND THERMODYNAMIC PROPERTIES OF THE TEST FLUIDS

In order to solve the differential equations which give the theoretical pressure profile, it was necessary to express certain fluid properties as a function of temperature. Jaeger (1966) has shown that, from free energy considerations, it is justifiable to assume that the condensate may exist as a supercooled liquid below the triple point, and that liquid properties may be extrapolated into this range.

For surface tension, density and heat of vaporization, the most convenient means of expressing the data was as a linear function of temperature:

$$X_t = X_o - At \tag{E.1}$$

where X_t is the property at temperature t

X_o is the property at 0°C.

A is a constant

t is the temperature in °C.

For vapor pressure, the data above the triple point was expressed as:

$$\log_{10}(p_{sat}) = -B/T + C \tag{E.2}$$

where B and C are constants

T is the absolute temperature in °K.

Below the triple point, the Clausius-Clapeyron relation between saturation properties was used as a means of extrapolating the vapor pressure:

$$\frac{h_{fg}}{v_{fg}} = (T)\,\frac{dp_\infty}{dT}$$

But since pv = RT for a perfect gas, and $v_{fg} \cong v$:

$$\frac{dp_\infty}{p_\infty} = \frac{h_{fg}}{R}\,\frac{dT}{T^2}$$

Integrating, with $h_{fg} = (h_{fg})_{t=0} - A_2 t = (h_{fg})_{T=0} - A_2 T$,

$$\ell n \frac{p_\infty}{(p_\infty)_{T.P.}} = \frac{(h_{fg})_{T=0}}{RT} + \frac{(h_{fg})_{T=0}}{RT_{T.P.}} - \frac{A_2}{R} \ell n \frac{T}{T_{T.P.}} \qquad (E.3)$$

The constants involved in the above equations for benzene and chloroform are given on the following two pages.

BENZENE

DENSITY: From Figure E-1, $\rho = \rho_o - A_1 t$

where ρ_o = 0,900 gm/cc and A_1 = .00108 gm/cc - °C.

References: International Critical Tables, Vol. 3 (1928).

Kuss (1955).

HEAT OF VAPORIZATION: From Figure E-2, $h_{fg} = (h_{fg})_{t=0} - A_2 t$

where $(h_{fg})_{t=0}$ = 194.0 BTU/lbm and A_2 = 0.310 BTU/lbm -°C.

References: International Critical Tables, Vol. 5 (1928).

Gottschall and Korvezee (1953).

SURFACE TENSION: From Figure E-3, $\sigma = \sigma_o - A_3 t$

where σ_o = 31.7 dyne/cm and A_3 = 0.129 dyne/cm - °C.

References: International Critical Tables, Vol. 4 (1928).

Metzger (1946).

VAPOR PRESSURE: Above the triple point, $\log_{10}(p_\infty) = -\frac{B}{T} + C$

where p_∞ is the vapor pressure in mm of mercury, B = 1785, C = 7.9622

Reference: Handbook of Chemistry and Physics, 43rd Edition.

Below the triple point the Clausius-Clapeyron relation (Equation E.3) is used, where

$p_{T.P.}$ = 34. 9 mm of mercury

$T_{T.P.}$ = 5,5 °C. ≃ 278 °K.

$(h_{fg})_{T=0}$ = 278.6 BTU/lbm

A_2 = 0.130 BTU/lbm - °K.

R = .0457 BTU/lbm - °K.

CHLOROFORM

DENSITY: From Figure E-4, $\rho = \rho_o - A_1 t$

where ρ_o = 1.526 gm/cc and A_1 = .00186 gm/cc - °C.

References: International Critical Tables, Vol. 3 (1928).

Physico-Chemical Constants of Pure Organic Compounds.

HEAT OF VAPORIZATION: From Figure E-5, $h_{fg} = (h_{fg})_{t=0} - A_2 t$

where $(h_{fg})_{t=0}$ = 116.8 BTU/lbm and A_2 = 0.174 BTU/lbm - °C.

References: International Critical Tables, Vol. 5 (1928).

Physico-Chemical Constants of Pure Organic Compounds.

SURFACE TENSION: From Figure E-6, $\sigma = \sigma_o - A_3 t$

where σ_o = 30.0 dyne/cm and A_3 = 0.137 dyne/cm - °C.

References: International Critical Tables, Vol. 4 (1928).

Physico-Chemical Constants of Pure Organic Compounds.

VAPOR PRESSURE: Above the triple point, a best line through the data in Figure E-7 gives a relation similar to Equation E.2,

where p_∞ is the vapor pressure in mm of mercury, B = 1770, C = 8.24

References: Handbook of Chemistry and Physics, 43rd Edition.

International Critical Tables, Vol. 3 (1928).

Below the triple point the Clausius-Clapeyron relation (Equation E.3) is used, where

$p_{T.P.}$ = 0.646 mm of mercury

$T_{T.P.}$ = -63.5 °C. ≈ 210 °K.

$(h_{fg})_{T=0}$ = 164.3 BTU/lbm

A_2 = 0.174 BTU/lbm - °K.

R = .0299 BTU/lbm - °K

FIGURE E-1 DENSITY OF LIQUID BENZENE VS. TEMPERATURE

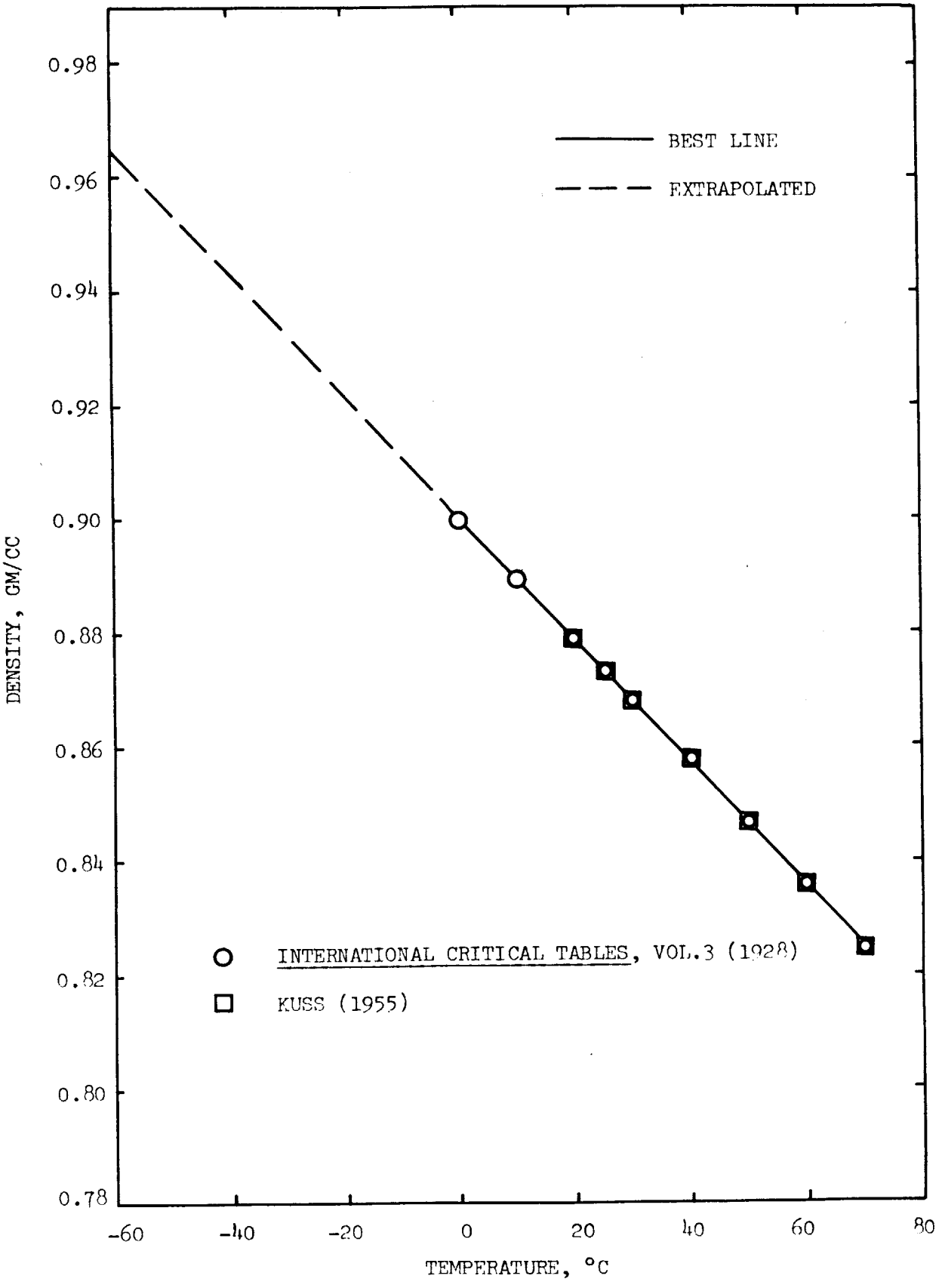

FIGURE E-2 HEAT OF VAPORIZATION OF BENZENE VS. TEMPERATURE

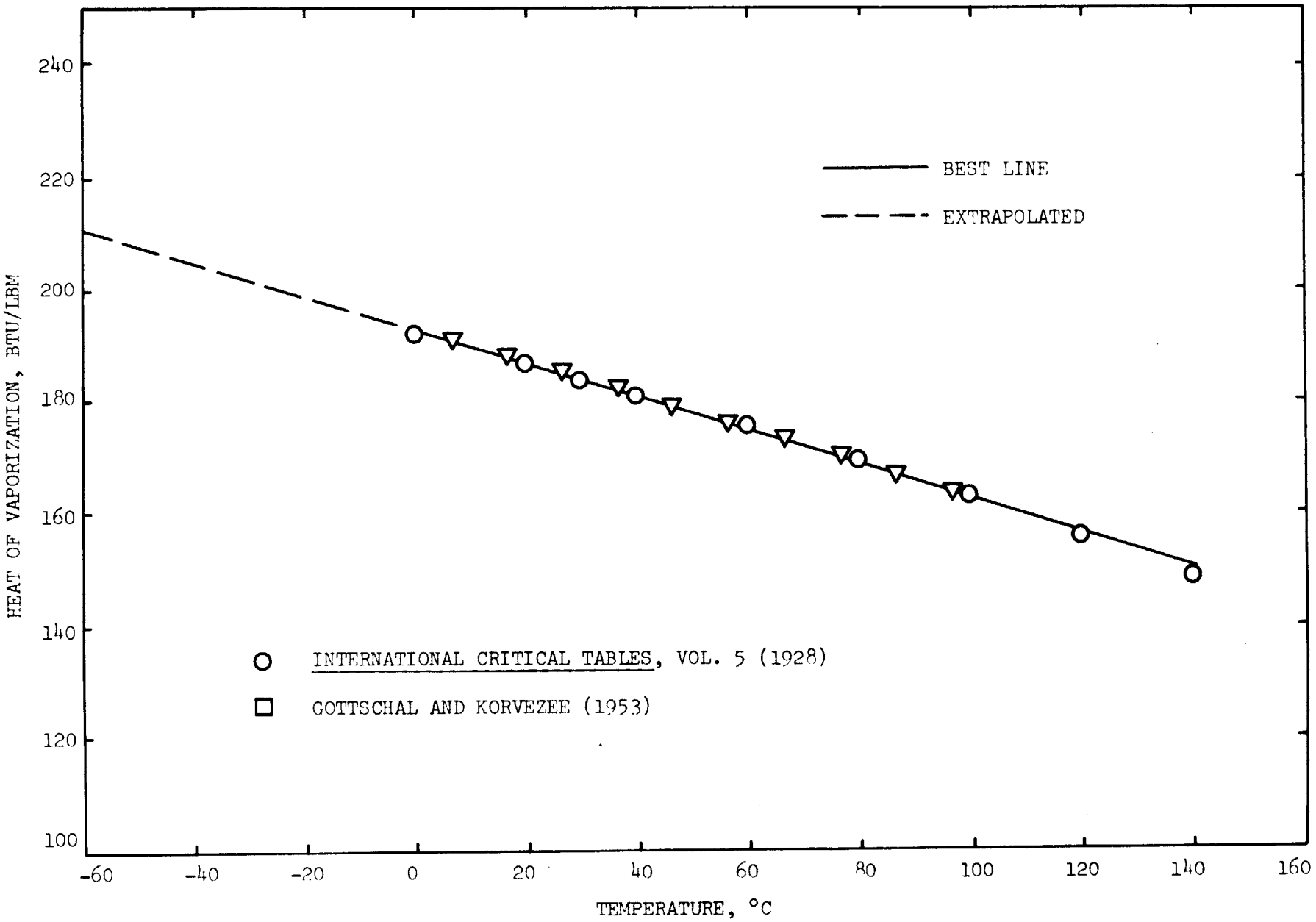

FIGURE E-3 SURFACE TENSION OF BENZENE IN THE PRESENCE OF ITS OWN VAPOR

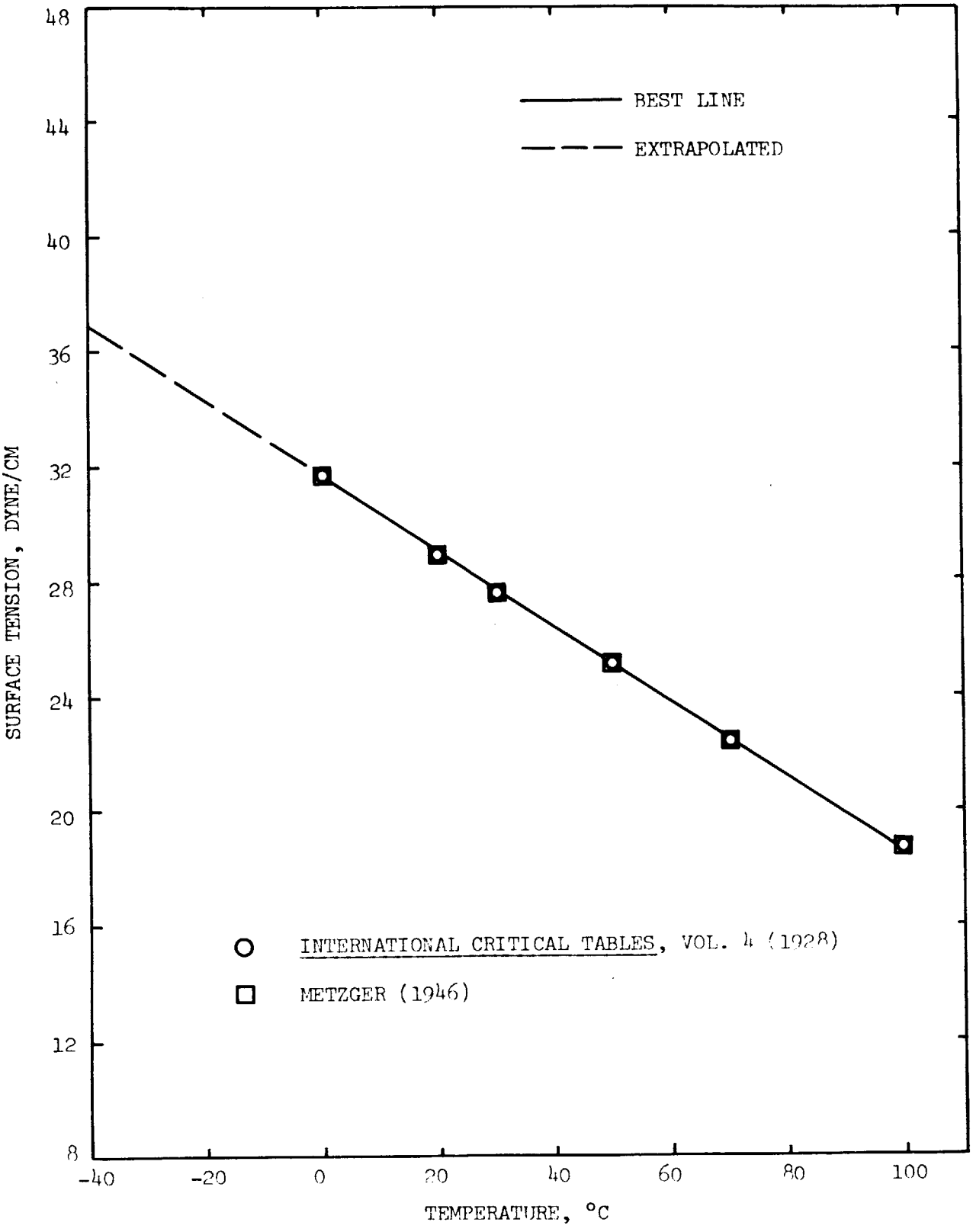

FIGURE E-4 DENSITY OF LIQUID CHLOROFORM VS. TEMPERATURE

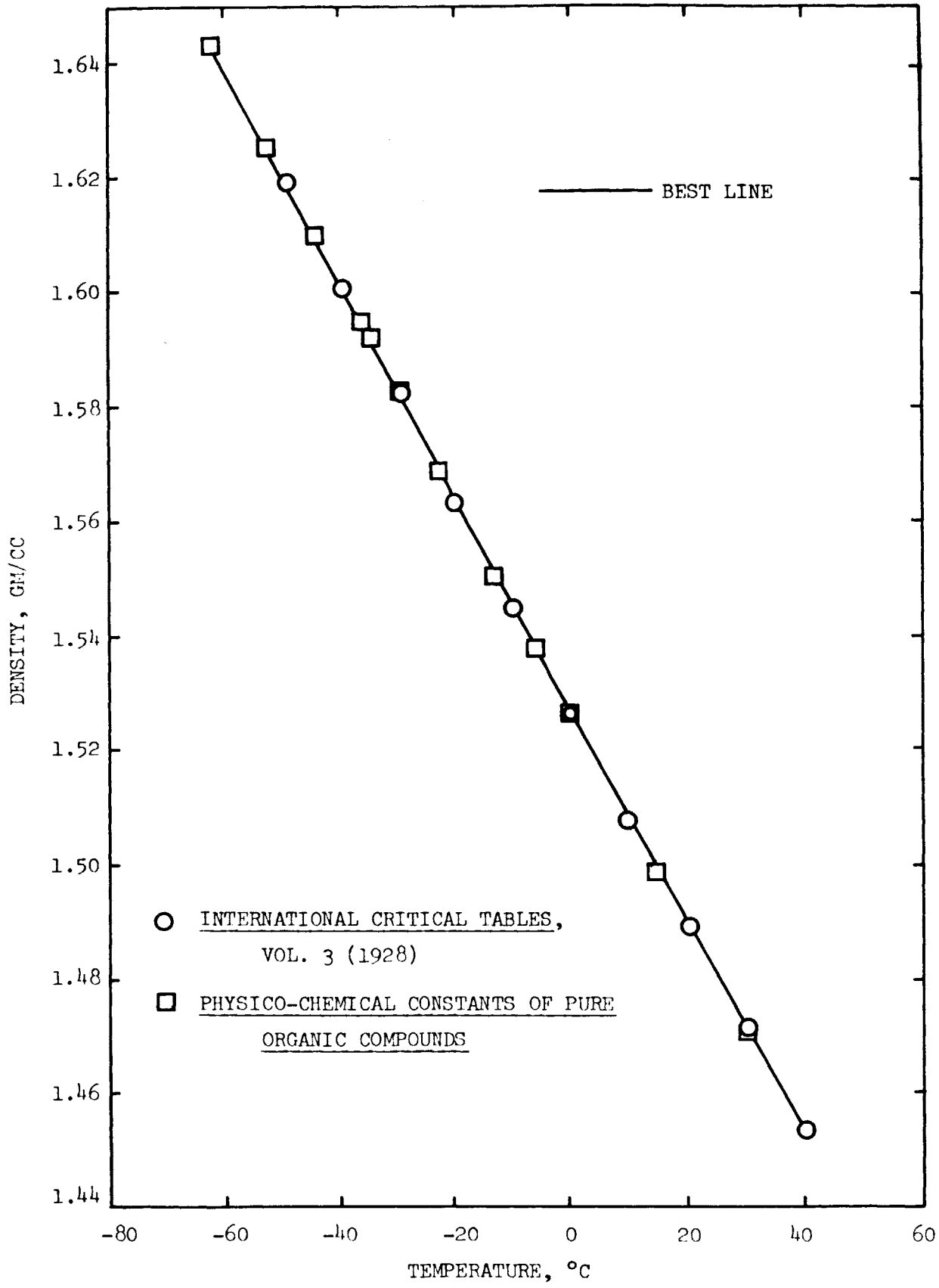

FIGURE E-5 HEAT OF VAPORIZATION OF CHLOROFORM VS. TEMPERATURE

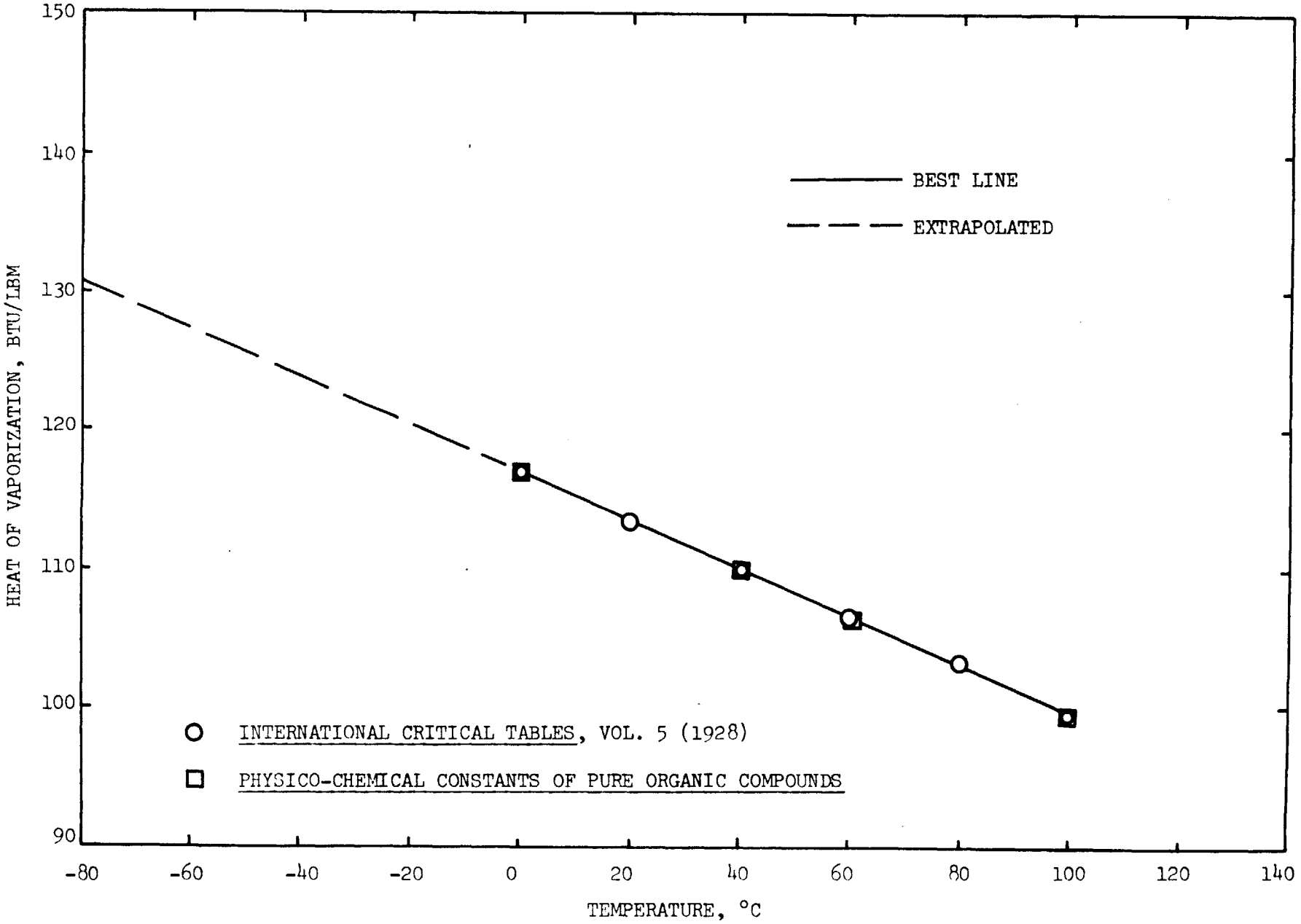

FIGURE E-6 SURFACE TENSION OF CHLOROFORM IN THE PRESENCE OF ITS OWN VAPOR

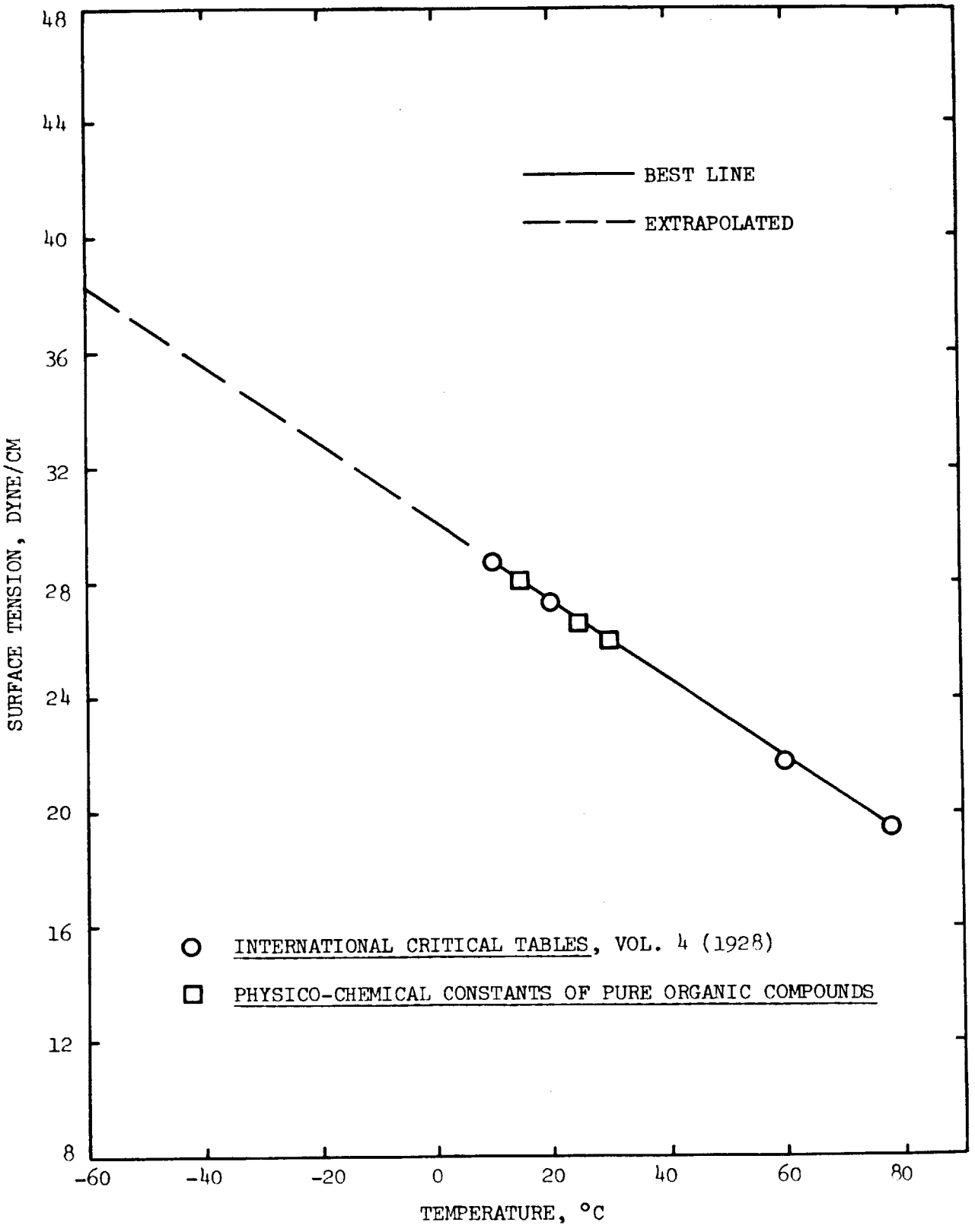

FIGURE E-7 CHLOROFORM VAPOR PRESSURE VS. RECIPROCAL TEMPERATURE (1/T)

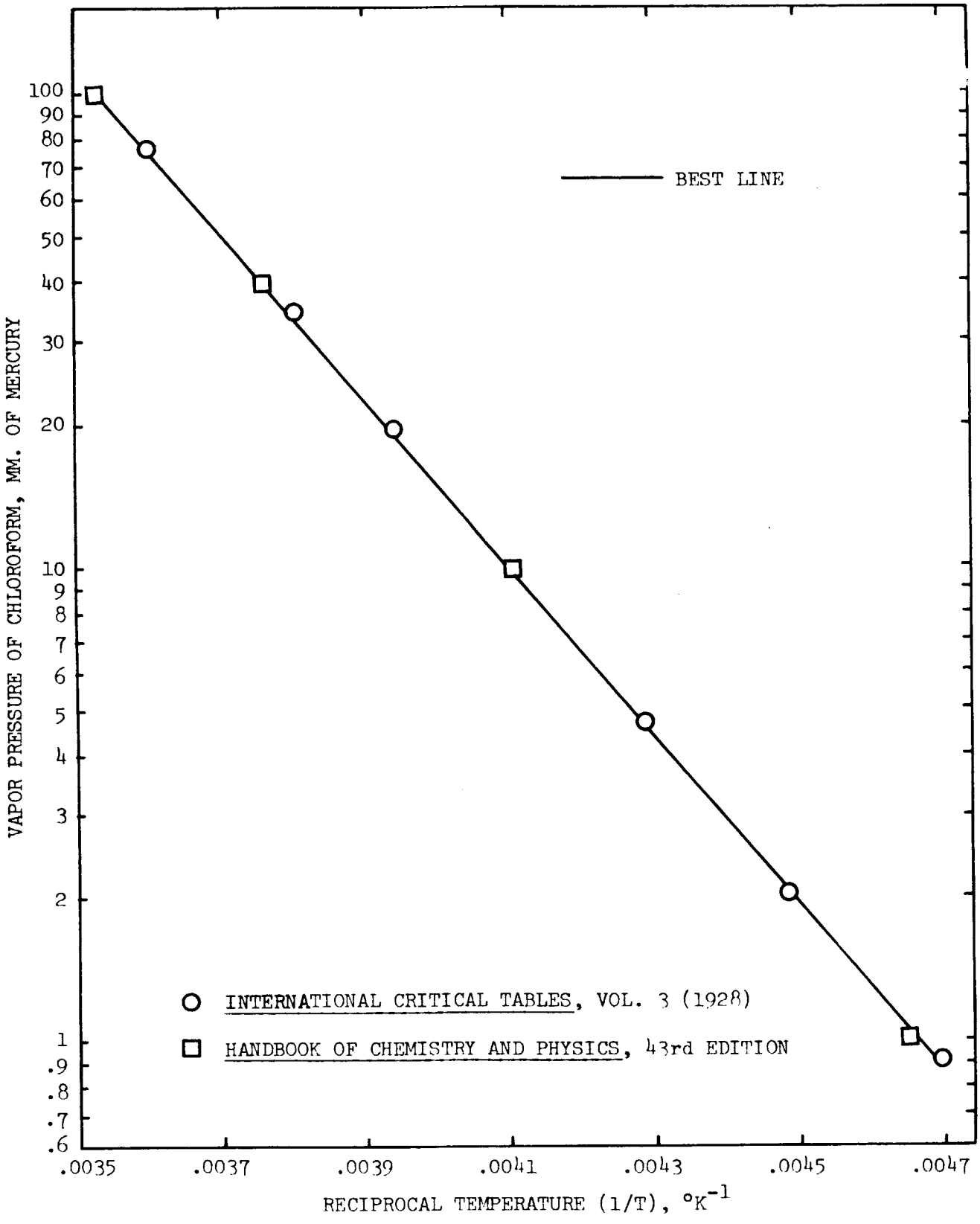

APPENDIX F TABULATION OF EXPERIMENTAL DATA

The measured values of P/P_o for each experiment are tabulated in this appendix. Measurements were made at a total of nineteen taps.

For each experiment, there is a corresponding pressure distribution obtained with dry air alone which may be used to define the effective area distribution of the nozzle by equation (2), with $\gamma = 1.4$. In Table F-1, there are tabulated eight sets of dry air data, numbered I through VIII. For each, the test numbers to which it corresponds are indicated. There are two reasons for the differences in the pressure distributions. First, each time the nozzle was disassembled, and reassembled after cleaning, the pressure distribution would change because it was impossible either to reset the angle between the top and bottom plates or to tighten the set screws exactly as they had been before. Secondly, there was a buildup of dirt and fluid on the nozzle walls after a period of time which might have disturbed the flow or changed the effective flow area near certain pressure taps.

The effect of reassembling the nozzle may be seen in the small difference in the pressure distribution exhibited by Isentrope VI compared to Isentropes I through V, and in the larger change shown by Isentropes VII and VIII compared to previous data. Other differences may be due either to experimental error or to the effect of the buildup on the nozzle walls. Experimental error should not have produced a change in P/P_o greater than $\pm$ .001 so the error due to buildup would appear to be significant. This is supported by the observation that the experimental data with benzene and chloroform was, in general, consistent with the corresponding dry air isentrope.

The experimental data for benzene is shown in Table F-2, and data for chloroform is shown in Table F-3. Data for selected tests from both these tables is plotted versus A/A^* (effective area ratio) in Figures 4 through 11 in the body of the report.

TABLE F-1 TABULATION OF DRY AIR DATA

Isentrope No.	I	II	III	IV	V	VI	VII	VIII
P_o (atm.) =	3.97	3.93	3.96	3.93	3.66	3.64	3.61	3.66
T_o (^oF) =	93	90	108	85	93	91	91	70
Test Nos.	1-5	6-9	10-17	18-30	31-38	39-43	44-57	58-67
X, in.	P/P_o	P/P_o	P/P_o	P/P_o	P/P_o	P/P_o	P/P_o	P/P_o
0.2	.358	.360	.360	.357	.357	.356	.375	.377
0.3	.310	.313	.314	.310	.310	.308	.323	.322
0.4	.274	.277	.274	.268	.271	.267	.281	.282
0.5	.247	.250	.250	.247	.247	.244	.252	.256
0.6	.225	.226	.223	.222	.223	.220	.230	.233
0.7	.201	.205	.204	.201	.203	.200	.208	.211
0.8	.186	.187	.186	.185	.186	.184	.190	.192
0.9	.170	.172	.172	.169	.171	.168	.175	.177
1.0	.157	.158	.159	.156	.156	.153	.163	.165
1.1	.148	.149	.149	.147	.149	.144	.153	.154
1.2	.140	.139	.140	.139	.139	.136	.143	.143
1.3	.131	.133	.133	.130	.131	.129	.135	.136
1.4	.123	.123	.124	.122	.122	.119	.125	.127
1.5	.113	.114	.114	.112	.113	.111	.117	.118
1.6	.109	.109	.109	.108	.109	.107	.113	.114
1.7	.106	.106	.106	.104	.105	.104	.108	.110
1.8	.100	.100	.101	.099	.099	.098	.102	.102
1.9	.096	.096	.096	.094	.094	.093	.098	.098
2.0	.092	.092	.092	.090	.091	.089	.093	.094

TABLE F-2 TABULATION OF BENZENE DATA

Test No.	1	2	3	4	5	6	7	8	9
P_o (atm.) =	3.99	4.00	4.03	4.02	4.02	4.02	4.02	4.02	4.03
T_o (°F) =	108	113	116	119	121	121	138	138	136
ω_o =	.063	.080	.087	.096	.104	.080	.087	.079	.116
X, in.	P/P_o	P/P_o	P/P_o	P/P_o	P/P_o	P/P_o	P/P_o	P/P_o	P/P_o
0.2	.360	.362	.360	.363	.364	.362	.363	.364	.364
0.3	.312	.313	.313	.316	.316	.316	.317	.318	.318
0.4	.274	.275	.277	.280	.281	.278	.278	.279	.279
0.5	.249	.250	.250	.253	.256	.253	.254	.255	.255
0.6	.230	.234	.233	.236	.237	.229	.228	.228	.229
0.7	.214	.220	.219	.224	.228	.215	.212	.213	.218
0.8	.205	.210	.209	.213	.217	.201	.198	.200	.206
0.9	.197	.203	.204	.208	.207	.197	.194	.196	.205
1.0	.185	.190	.192	.195	.197	.188	.187	.191	.196
1.1	.177	.182	.183	.186	.188	.181	.182	.185	.188
1.2	.165	.170	.171	.175	.176	.169	.172	.174	.177
1.3	.155	.159	.161	.164	.165	.159	.162	.164	.165
1.4	.145	.150	.151	.154	.155	.148	.151	.153	.156
1.5	.136	.140	.142	.145	.146	.140	.143	.145	.147
1.6	.132	.135	.136	.139	.140	.135	.138	.140	.141
1.7	.127	.129	.130	.133	.134	.129	.133	.134	.136
1.8	.117	.121	.123	.125	.126	.122	.124	.126	.127
1.9	.112	.114	.116	.118	.120	.115	.118	.120	.121
2.0	.108	.111	.112	.115	.116	.111	.114	.116	.117

TABLE F-2 Cont.

Test No.	10	11	12	13	14	15	16	17	18
P_o (atm.) =	3.97	4.01	4.01	4.01	4.01	4.01	4.01	3.77	3.98
T_o (^oF) =	121	120	138	138	120	138	139	138	103
ω_o =	.074	.094	.096	.109	.092	.094	.087	.086	.034
X, in.	P/P_o	P/P_o	P/P_o	P/P_o	P/P_o	P/P_o	P/P_o	P/P_o	P/P_o
0.2	.361	.362	.363	.364	.363	.362	.362	.364	.363
0.3	.316	.316	.317	.318	.317	.317	.317	.319	.316
0.4	.277	.277	.277	.279	.278	.278	.278	.279	.275
0.5	.252	.254	.255	.256	.254	.254	.253	.256	.251
0.6	.228	.231	.229	.230	.230	.228	.227	.229	.225
0.7	.214	.219	.211	.215	.218	.210	.209	.211	.206
0.8	.201	.208	.195	.201	.206	.195	.191	.196	.188
0.9	.198	.205	.190	.200	.204	.189	.183	.191	.175
1.0	.190	.196	.186	.194	.195	.184	.176	.185	.164
1.1	.181	.186	.181	.186	.186	.180	.173	.181	.156
1.2	.168	.174	.170	.175	.174	.169	.165	.171	.147
1.3	.159	.164	.162	.165	.164	.161	.159	.162	.144
1.4	.150	.152	.151	.154	.152	.150	.148	.152	.134
1.5	.139	.144	.143	.146	.144	.143	.141	.145	.126
1.6	.134	.137	.139	.141	.138	.138	.136	.139	.121
1.7	.129	.132	.133	.135	.133	.133	.131	.133	.118
1.8	.120	.124	.125	.126	.126	.125	.123	.126	.111
1.9	.114	.117	.118	.120	.118	.118	.117	.119	.104
2.0	.111	.114	.114	.116	.115	.114	.113	.114	.101

TABLE F-2 Cont.

Test No.	19	20	21	22	23	24	25	26	27
P_o (atm.) =	3.74	3.95	3.94	3.94	3.94	4.02	4.02	4.03	4.03
T_o (°F) =	138	97	100	102	103	89	92	94	97
ω_o =	.037	.038	.044	.049	.053	.032	.036	.040	.043
X, in.	P/P_o	P/P_o	P/P_o	P/P_o	P/P_o	P/P_o	P/P_o	P/P_o	P/P_o
0.2	.360	.356	.356	.356	.356	.356	.355	.356	.356
0.3	.312	.308	.309	.309	.311	.309	.310	.309	.311
0.4	.274	.268	.269	.269	.269	.269	.270	.270	.271
0.5	.249	.246	.246	.247	.247	.246	.247	.247	.249
0.6	.225	.223	.223	.225	.225	.223	.222	.224	.225
0.7	.205	.202	.203	.205	.208	.203	.203	.204	.206
0.8	.188	.186	.187	.192	.195	.188	.189	.190	.192
0.9	.173	.172	.176	.183	.186	.175	.178	.179	.182
1.0	.158	.162	.166	.174	.175	.165	.167	.170	.171
1.1	.152	.156	.160	.166	.169	.159	.161	.163	.167
1.2	.142	.148	.152	.157	.158	.150	.152	.153	.156
1.3	.137	.144	.145	.147	.149	.144	.144	.145	.147
1.4	.129	.135	.138	.139	.140	.135	.136	.138	.138
1.5	.121	.125	.129	.132	.133	.126	.128	.129	.131
1.6	.118	.121	.123	.126	.128	.121	.121	.124	.125
1.7	.114	.117	.119	.120	.121	.116	.116	.118	.119
1.8	.109	.111	.112	.114	.114	.110	.110	.111	.113
1.9	.104	.104	.106	.108	.108	.103	.105	.105	.106
2.0	.101	.101	.103	.103	.105	.100	.100	.102	.103

TABLE F-2 Cont.

Test No.	28	29	30	31	32	33	34	35	36
P_o (atm.) =	4.04	4.04	3.71	3.71	3.74	3.75	3.76	3.77	3.77
T_o (^oF) =	98	97	100	101	89	99	94	96	95
ω_o =	.046	.049	.057	.054	.044	.041	.037	.043	.046
X, in.	P/P_o	P/P_o	P/P_o	P/P_o	P/P_o	P/P_o	P/P_o	P/P_o	P/P_o
0.2	.356	.357	.358	.358	.358	.356	.359	.359	.359
0.3	.311	.311	.312	.313	.314	.311	.313	.313	.313
0.4	.271	.272	.272	.273	.273	.271	.272	.272	.272
0.5	.248	.249	.250	.250	.250	.247	.250	.250	.250
0.6	.226	.226	.227	.227	.227	.224	.226	.227	.227
0.7	.208	.209	.210	.209	.209	.205	.206	.208	.209
0.8	.194	.196	.197	.196	.196	.188	.189	.190	.193
0.9	.185	.187	.189	.188	.190	.177	.179	.181	.183
1.0	.174	.175	.179	.178	.175	.165	.166	.171	.173
1.1	.168	.170	.173	.171	.169	.162	.162	.165	.168
1.2	.156	.158	.162	.161	.157	.153	.152	.156	.157
1.3	.148	.149	.151	.151	.148	.145	.146	.147	.148
1.4	.139	.140	.143	.142	.140	.137	.137	.139	.139
1.5	.132	.132	.135	.134	.132	.130	.130	.132	.132
1.6	.127	.127	.131	.130	.126	.123	.124	.125	.127
1.7	.120	.122	.124	.124	.120	.119	.118	.120	.121
1.8	.113	.114	.116	.115	.113	.112	.111	.113	.114
1.9	.108	.108	.110	.110	.107	.106	.105	.107	.108
2.0	.104	.104	.107	.106	.104	.102	.102	.103	.104

TABLE F-2 Cont.

Test No.	37	38	39	40	41	42	43
P_o (atm.) =	3.77	3.77	3.65	3.65	3.65	3.65	3.64
T_o (^oF) =	96	97	94	94	94	95	96
ω_o =	.051	.054	.039	.044	.049	.054	.058
X, in.	P/P_o	P/P_o	P/P_o	P/P_o	P/P_o	P/P_o	P/P_o
0.2	.359	.359	.358	.358	.358	.357	.358
0.3	.313	.314	.308	.308	.309	.309	.309
0.4	.273	.273	.269	.269	.269	.269	.270
0.5	.251	.251	.245	.245	.245	.246	.246
0.6	.228	.229	.220	.222	.223	.223	.224
0.7	.210	.212	.201	.202	.203	.205	.208
0.8	.194	.198	.186	.188	.191	.194	.197
0.9	.187	.190	.174	.177	.182	.186	.190
1.0	.176	.179	.163	.167	.173	.176	.179
1.1	.170	.173	.156	.162	.166	.169	.171
1.2	.159	.161	.150	.154	.157	.159	.161
1.3	.149	.151	.144	.145	.147	.149	.150
1.4	.141	.142	.135	.138	.139	.140	.142
1.5	.133	.135	.126	.130	.132	.134	.135
1.6	.129	.130	.121	.124	.126	.128	.129
1.7	.123	.123	.117	.118	.120	.122	.122
1.8	.115	.115	.111	.112	.114	.114	.115
1.9	.108	.108	.104	.105	.107	.108	.108
2.0	.106	.106	.101	.102	.103	.104	.106

TABLE F-3 TABULATION OF CHLOROFORM DATA

Test No.	44	45	46	47	48	49	50	51	52
P_o (atm.) =	3.69	3.70	3.71	3.72	3.68	3.68	3.69	3.69	3.70
T_o (^oF) =	100	101	139	154	86	89	98	101	103
ω_o =	.142	.168	.176	.190	.043	.047	.050	.054	.058
X, in.	P/P_o	P/P_o	P/P_o	P/P_o	P/P_o	P/P_o	P/P_o	P/P_o	P/P_o
0.2	.379	.379	.382	.381	.375	.375	.375	.374	.373
0.3	.325	.326	.330	.329	.327	.327	.327	.329	.329
0.4	.286	.289	.287	.286	.283	.285	.285	.285	.289
0.5	.277	.282	.258	.259	.253	.254	.257	.257	.257
0.6	.283	.290	.237	.238	.231	.235	.236	.236	.235
0.7	.257	.257	.221	.217	.213	.214	.214	.216	.215
0.8	.230	.235	.209	.203	.203	.204	.201	.202	.204
0.9	.214	.215	.213	.194	.197	.197	.196	.198	.198
1.0	.197	.200	.199	.190	.178	.184	.187	.187	.190
1.1	.190	.191	.185	.186	.168	.172	.173	.175	.177
1.2	.175	.176	.174	.170	.156	.157	.159	.161	.162
1.3	.163	.166	.164	.164	.146	.150	.153	.154	.156
1.4	.153	.155	.153	.153	.138	.140	.142	.142	.143
1.5	.144	.146	.146	.144	.131	.134	.134	.136	.136
1.6	.139	.141	.141	.141	.125	.129	.132	.133	.132
1.7	.134	.135	.135	.134	.119	.122	.125	.126	.127
1.8	.124	.127	.126	.126	.112	.114	.115	.115	.117
1.9	.118	.120	.120	.120	.105	.107	.109	.110	.111
2.0	.115	.117	.117	.117	.100	.102	.105	.105	.106

TABLE F-3 Cont.

Test No.	53	54	55	56	57	58	59	60	61
P_o (atm.) =	3.70	3.70	3.70	3.70	3.70	3.71	3.71	3.72	3.74
T_o (^oF) =	105	107	108	110	110	138	139	140	140
ω_o =	.062	.066	.069	.073	.075	.132	.144	.155	.165
X, in.	P/P_o	P/P_o	P/P_o	P/P_o	P/P_o	P/P_o	P/P_o	P/P_o	P/P_o
0.2	.374	.373	.374	.375	.375	.380	.381	.381	.381
0.3	.328	.328	.328	.328	.328	.326	.328	.327	.326
0.4	.289	.288	.288	.288	.289	.286	.286	.288	.288
0.5	.258	.258	.259	.258	.260	.261	.262	.262	.263
0.6	.235	.238	.239	.242	.242	.239	.240	.240	.239
0.7	.214	.215	.217	.220	.221	.219	.220	.220	.221
0.8	.204	.206	.209	.211	.213	.205	.205	.207	.207
0.9	.199	.204	.205	.206	.208	.199	.202	.205	.208
1.0	.191	.191	.192	.194	.195	.202	.203	.207	.207
1.1	.181	.180	.181	.182	.182	.188	.190	.190	.190
1.2	.164	.166	.166	.167	.167	.170	.172	.175	.176
1.3	.157	.157	.157	.157	.158	.164	.167	.168	.169
1.4	.144	.145	.145	.145	.145	.153	.155	.153	.157
1.5	.139	.138	.138	.139	.140	.146	.148	.149	.150
1.6	.134	.134	.135	.136	.136	.142	.143	.145	.143
1.7	.129	.128	.128	.130	.130	.134	.135	.137	.137
1.8	.119	.119	.119	.119	.119	.125	.217	.128	.129
1.9	.111	.112	.112	.112	.113	.120	.121	.122	.123
2.0	.107	.108	.108	.108	.109	.115	.117	.118	.118

TABLE F-3 Cont.

Test No.	62	63	64	65	66	67
P_o (atm.) =	3.73	3.74	3.75	3.75	3.73	3.73
T_o (°F) =	137	137	137	137	103	107
ω_o =	.175	.185	.196	.205	.165	.200
X, in.	P/P_o	P/P_o	P/P_o	P/P_o	P/P_o	P/P_o
0.2	.381	.380	.380	.381	.380	.380
0.3	.326	.326	.326	.327	.326	.326
0.4	.289	.288	.288	.288	.287	.287
0.5	.264	.263	.263	.264	.270	.265
0.6	.239	.329	.240	.240	.264	.255
0.7	.222	.223	.223	.223	.274	.264
0.8	.211	.212	.211	.211	.235	.240
0.9	.216	.218	.217	.217	.221	.220
1.0	.207	.207	.207	.207	.202	.203
1.1	.191	.190	.190	.190	.194	.193
1.2	.178	.179	.179	.179	.183	.183
1.3	.170	.170	.169	.169	.170	.172
1.4	.159	.160	.159	.160	.159	.160
1.5	.151	.152	.152	.152	.149	.150
1.6	.145	.145	.145	.145	.143	.144
1.7	.138	.138	.137	.138	.139	.138
1.8	.129	.130	.130	.130	.130	.131
1.9	.124	.123	.123	.123	.123	.124
2.0	.120	.121	.120	.120	.119	.120

FIGURE 1 SCHEMATIC DIAGRAM OF APPARATUS

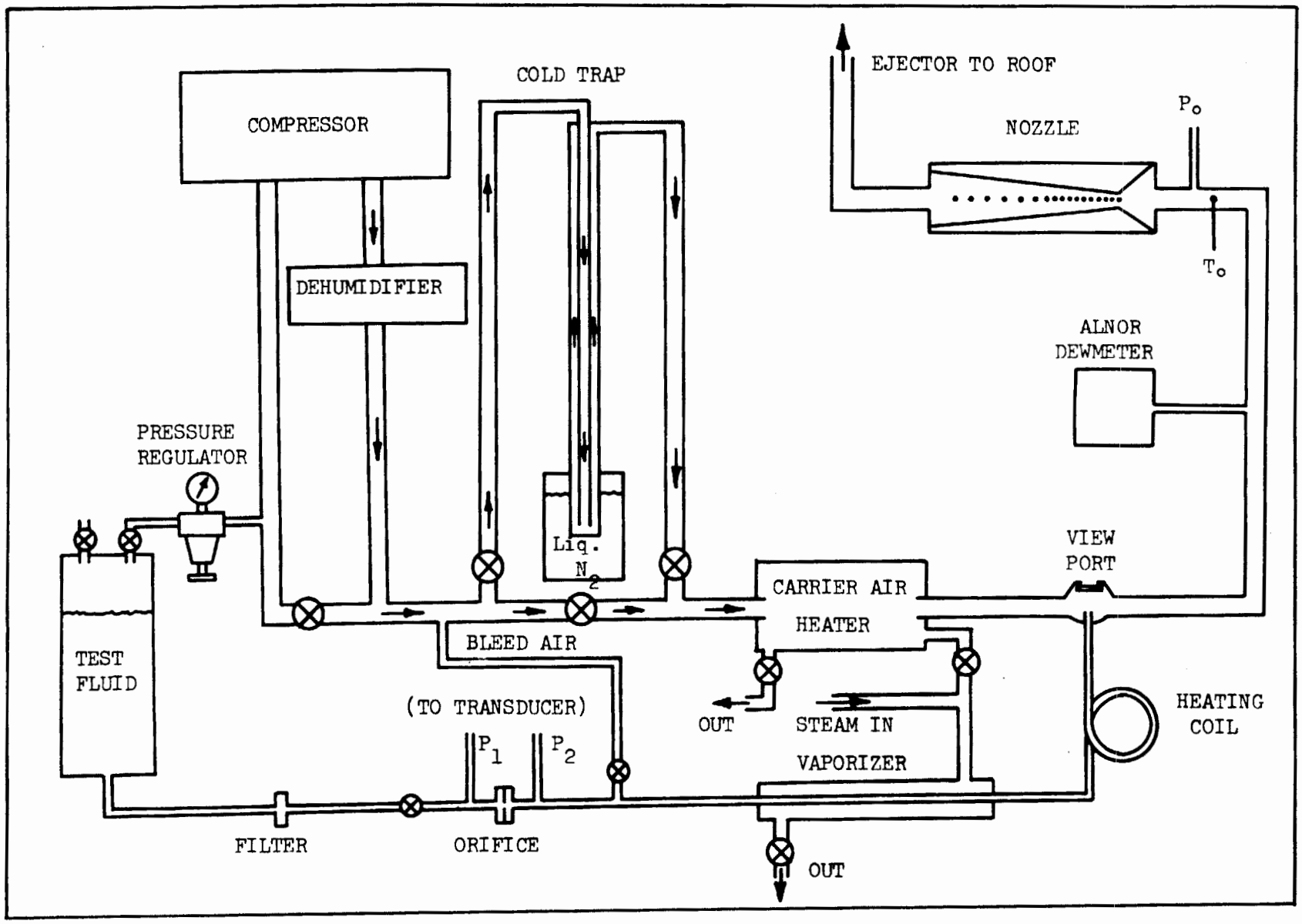

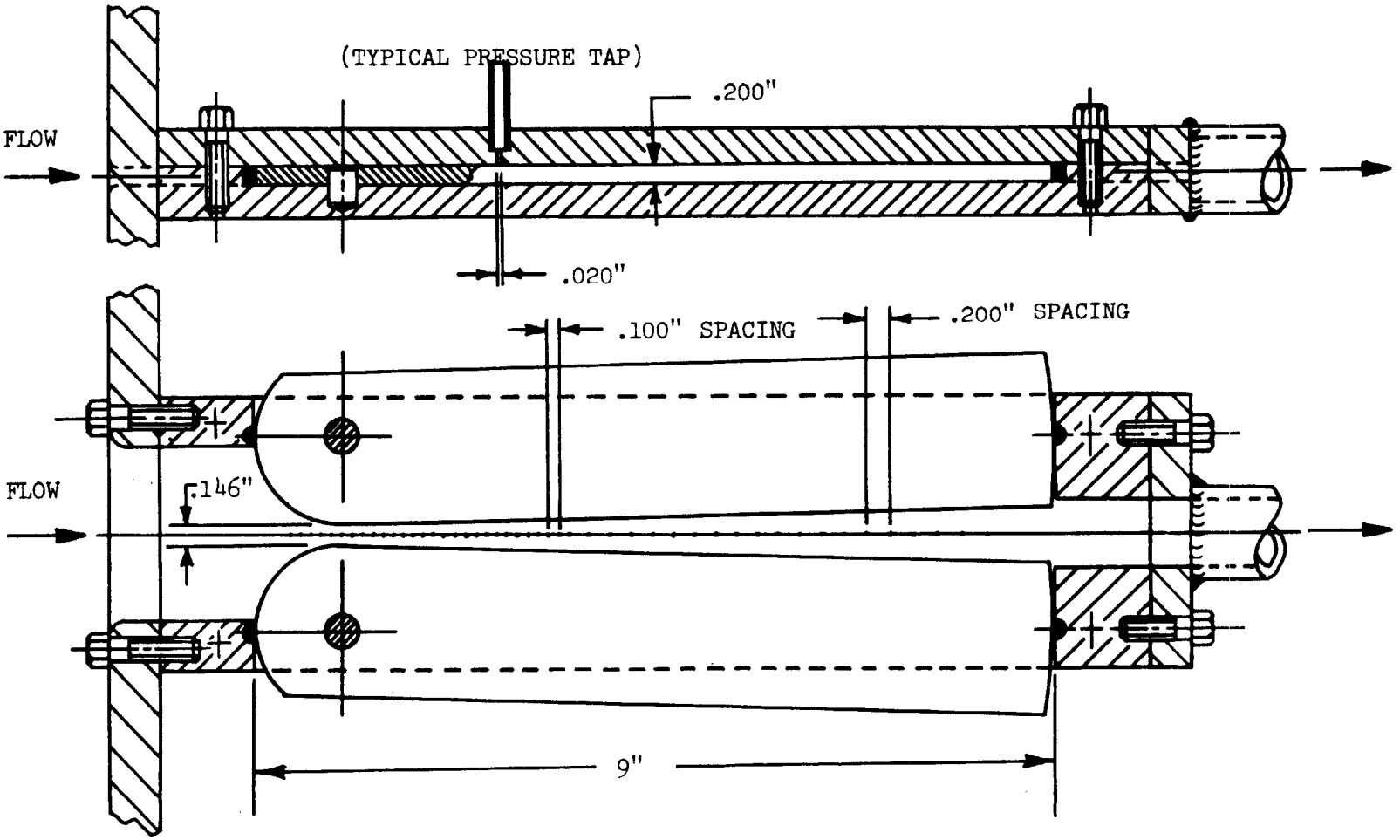

FIGURE 2 DETAIL OF NOZZLE II

FIGURE 3 EFFECTIVE AREA DISTRIBUTION OF NOZZLE II

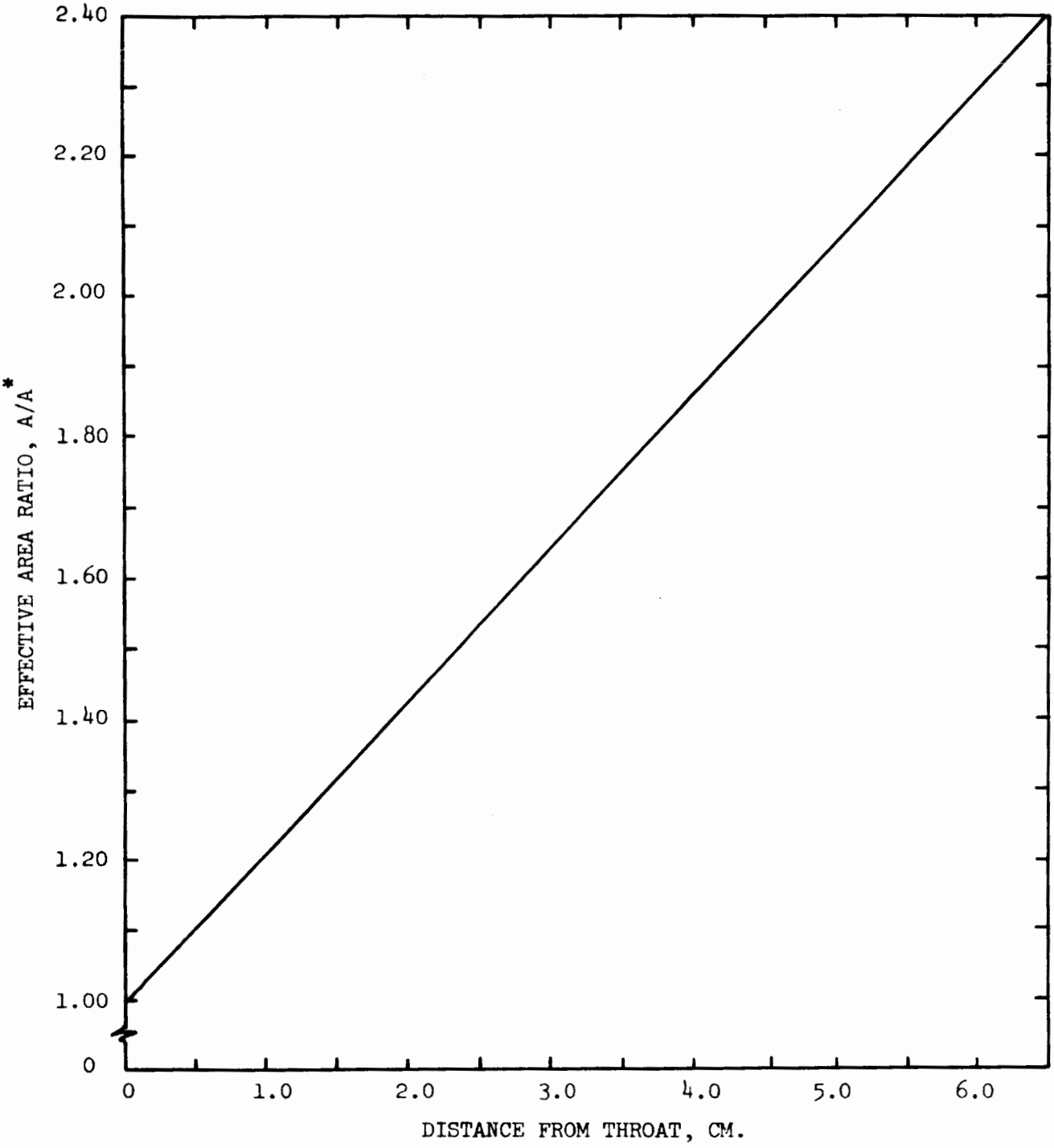

FIGURE 4 MASS-FLOW EFFECT ON PRESSURE PROFILES WITH BENZENE CONDENSATION

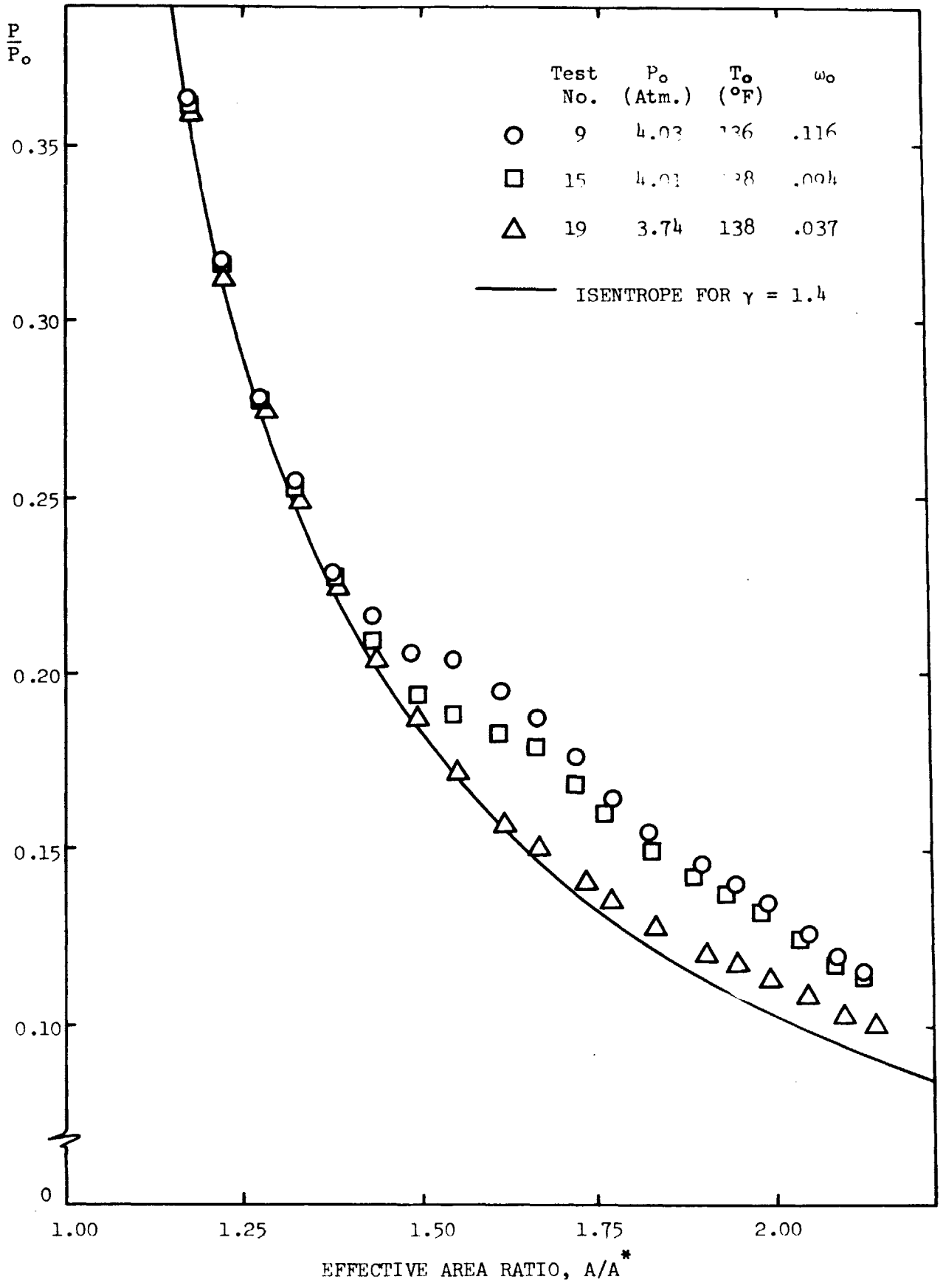

FIGURE 5 TEMPERATURE EFFECT ON PRESSURE PROFILES WITH BENZENE CONDENSATION

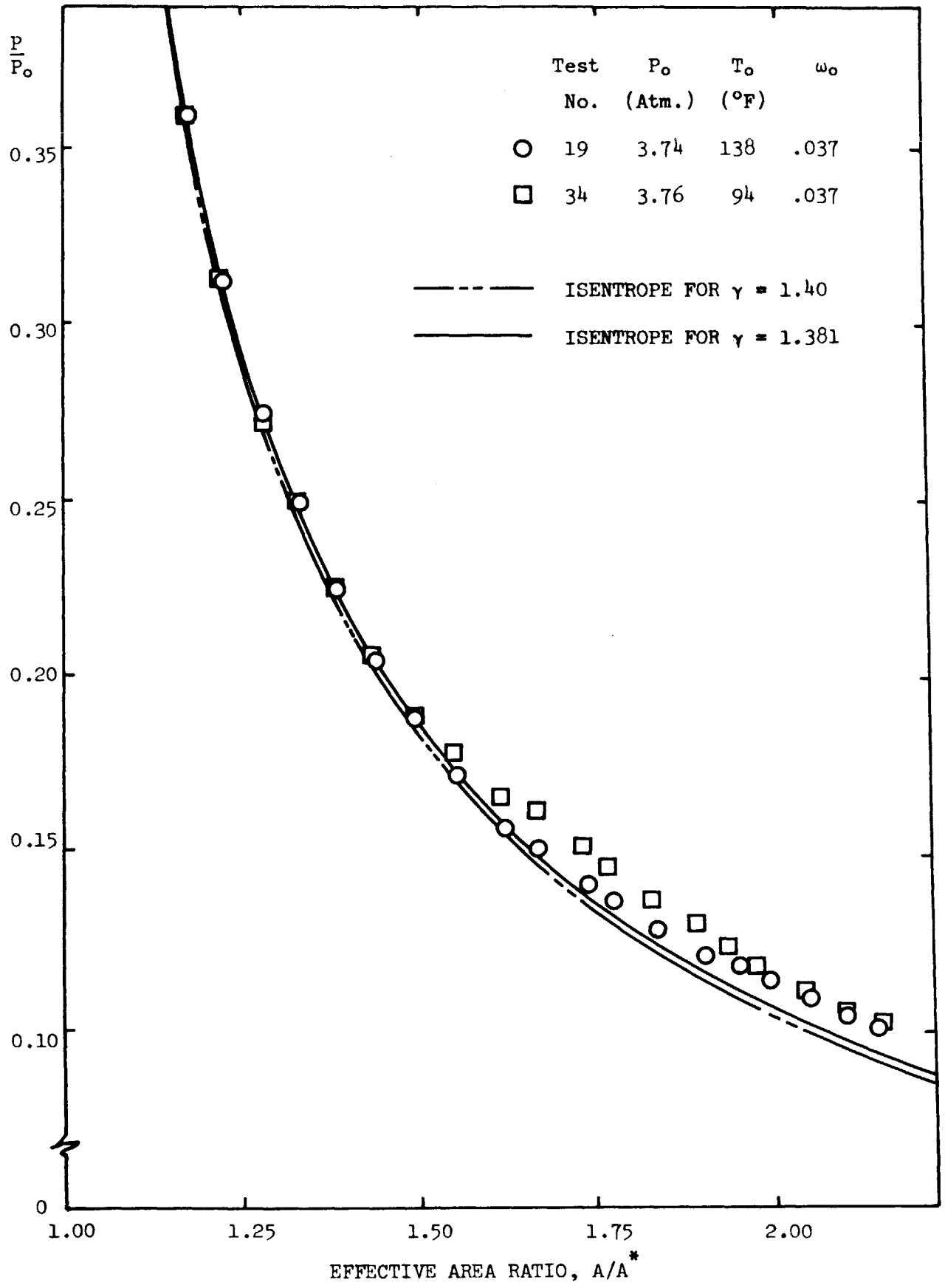

FIGURE 6 COMPARISON OF THEORY WITH DATA FOR BENZENE

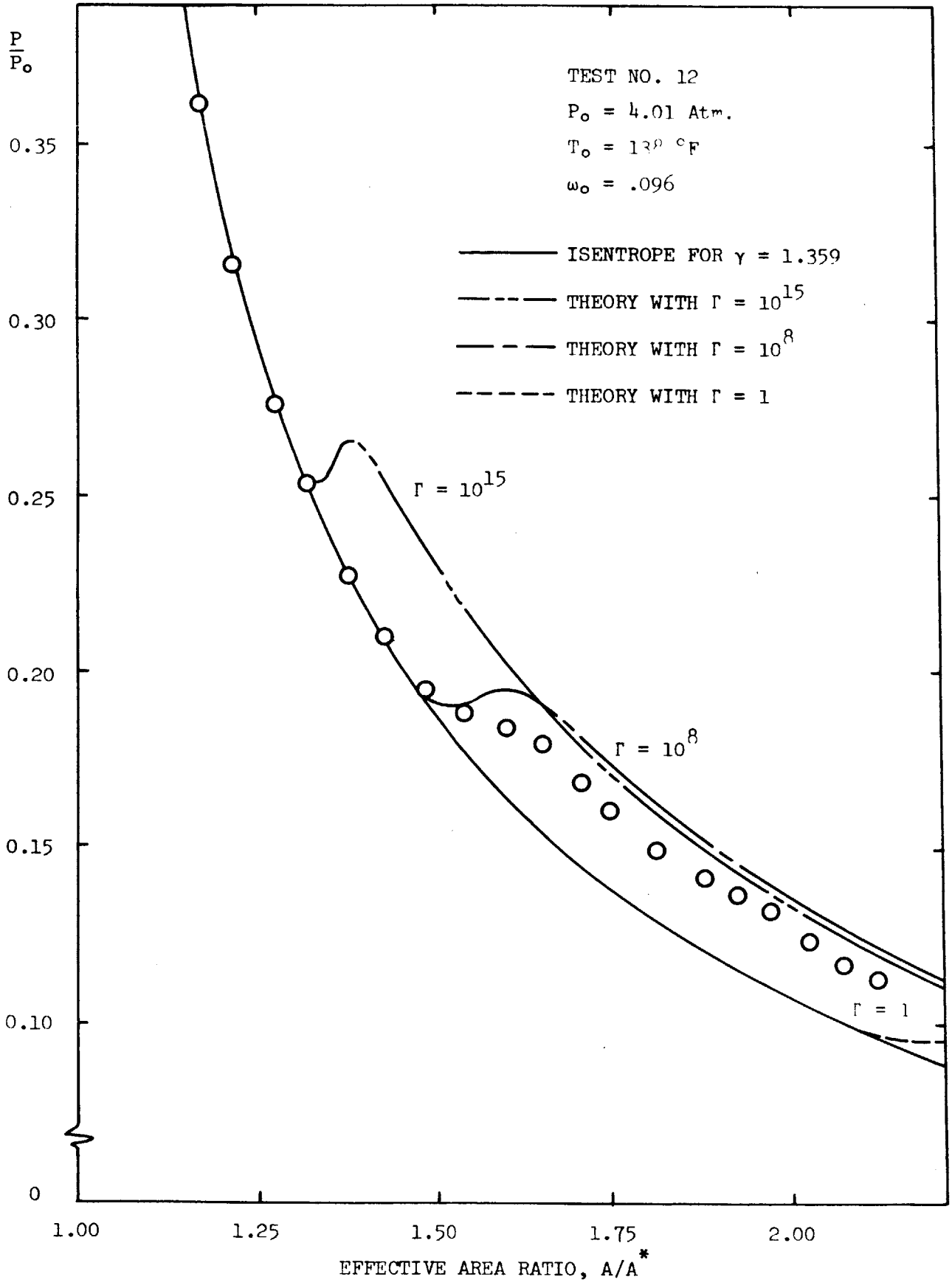

FIGURE 7 COMPARISON OF THEORY WITH DATA FOR BENZENE

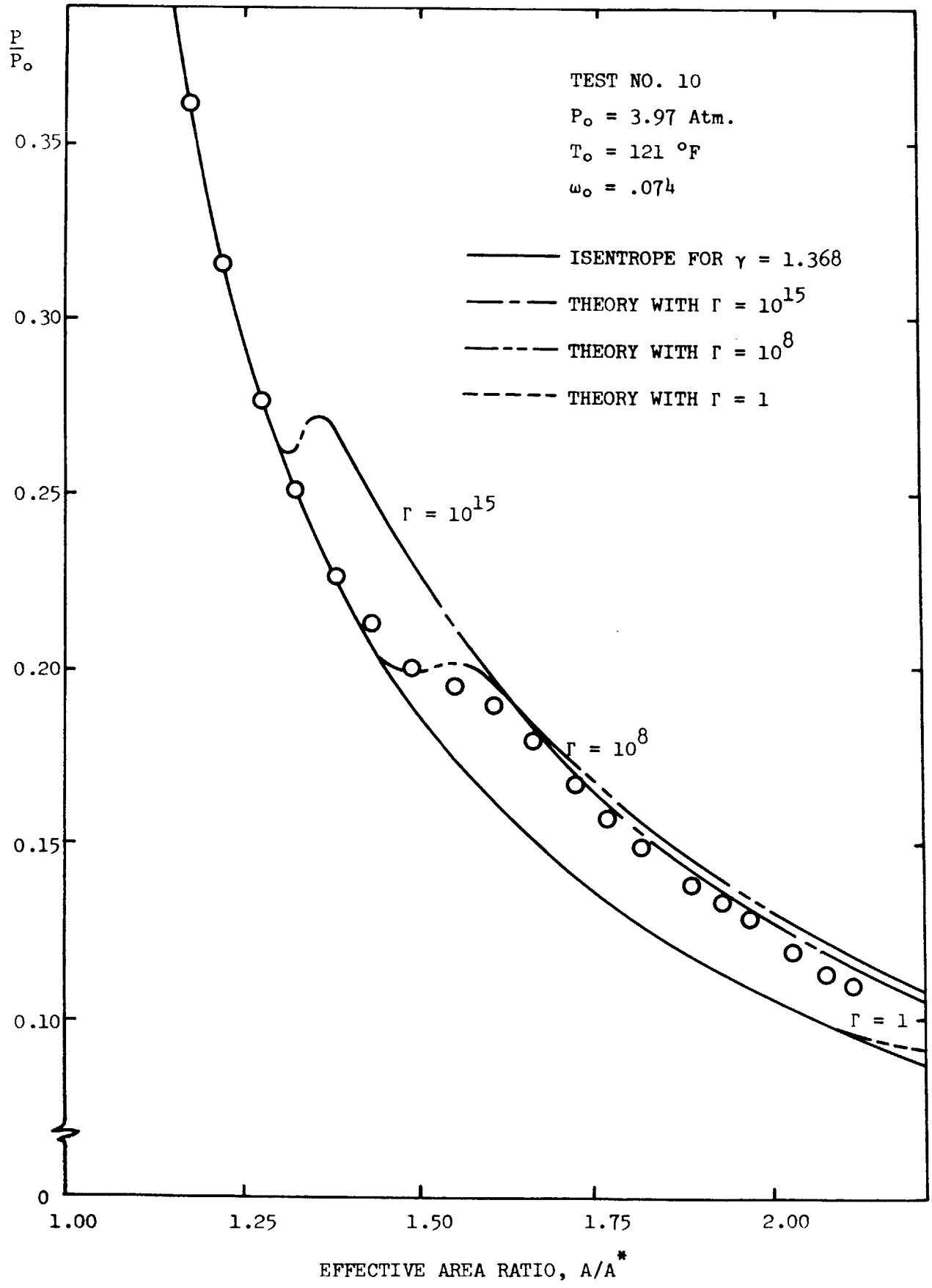

FIGURE 8a COMPARISON OF THEORY WITH DATA FOR BENZENE

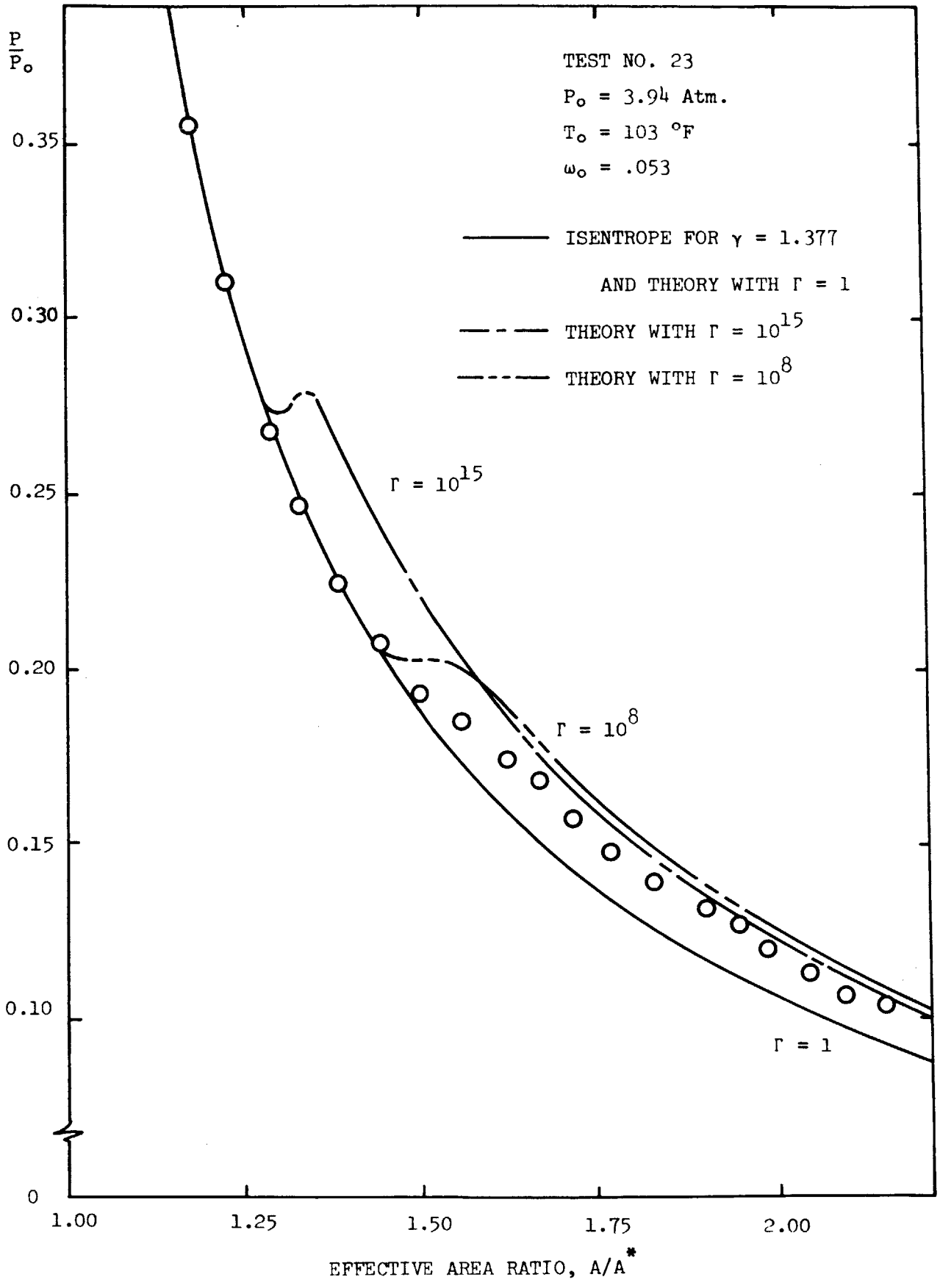

FIGURE 8b COMPARISON OF THEORY WITH DATA FOR BENZENE, EFFECT OF DECREASE IN SURFACE TENSION

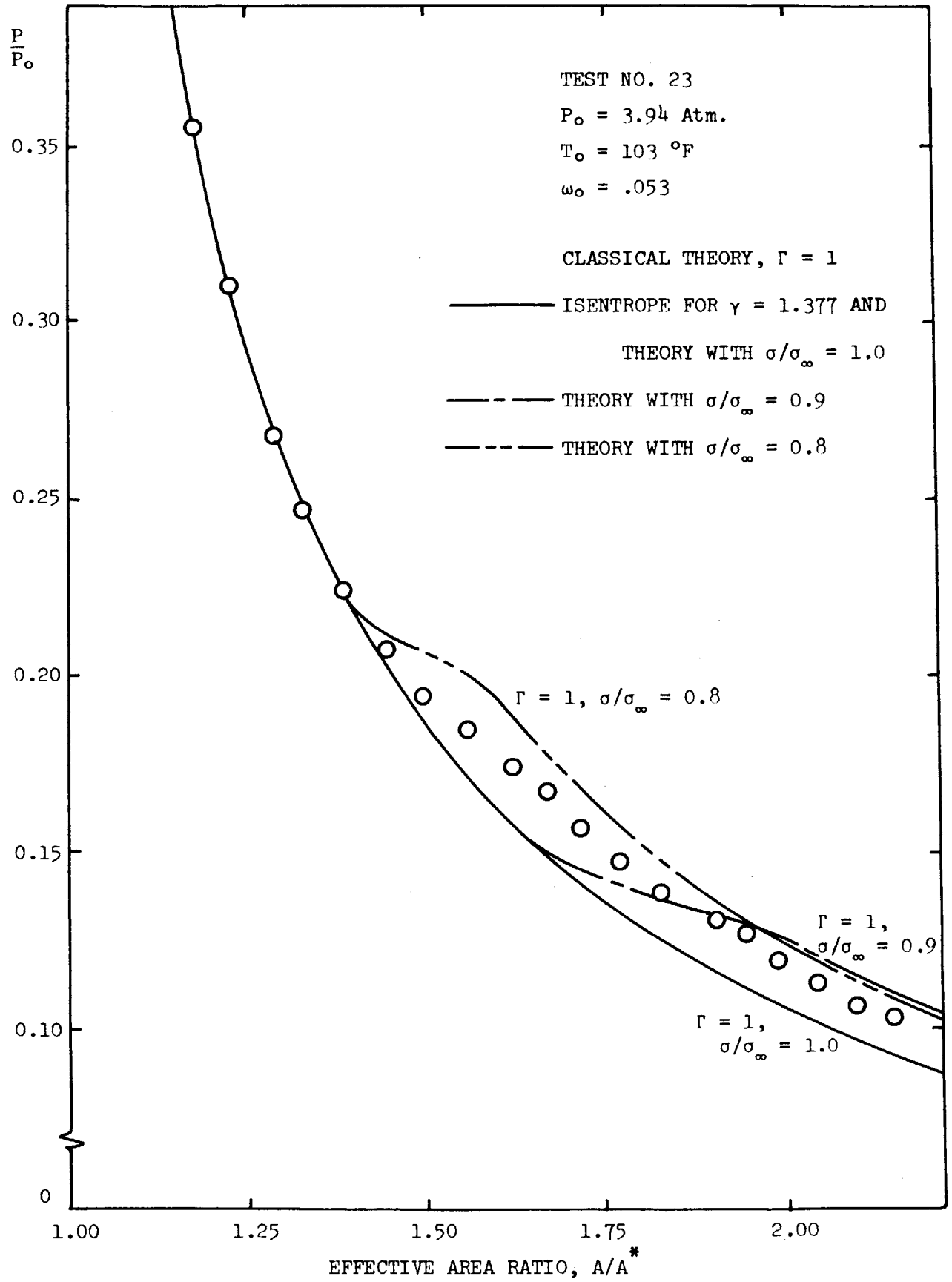

FIGURE 8c COMPARISON OF THEORY WITH DATA FOR BENZENE,
EFFECT OF INCREASE IN SURFACE TENSION

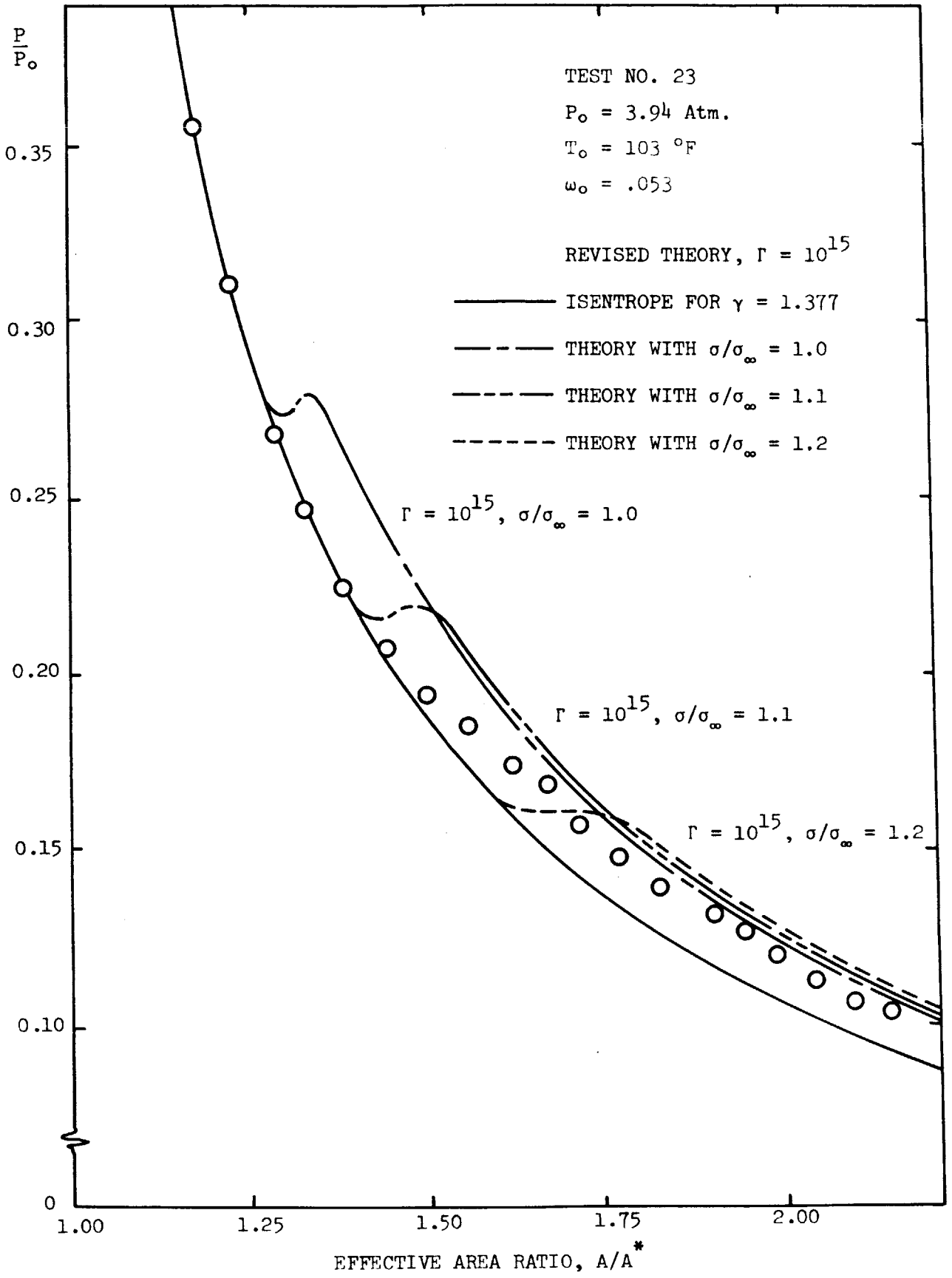

FIGURE 9 INCIDENCE OF BENZENE CONDENSATION

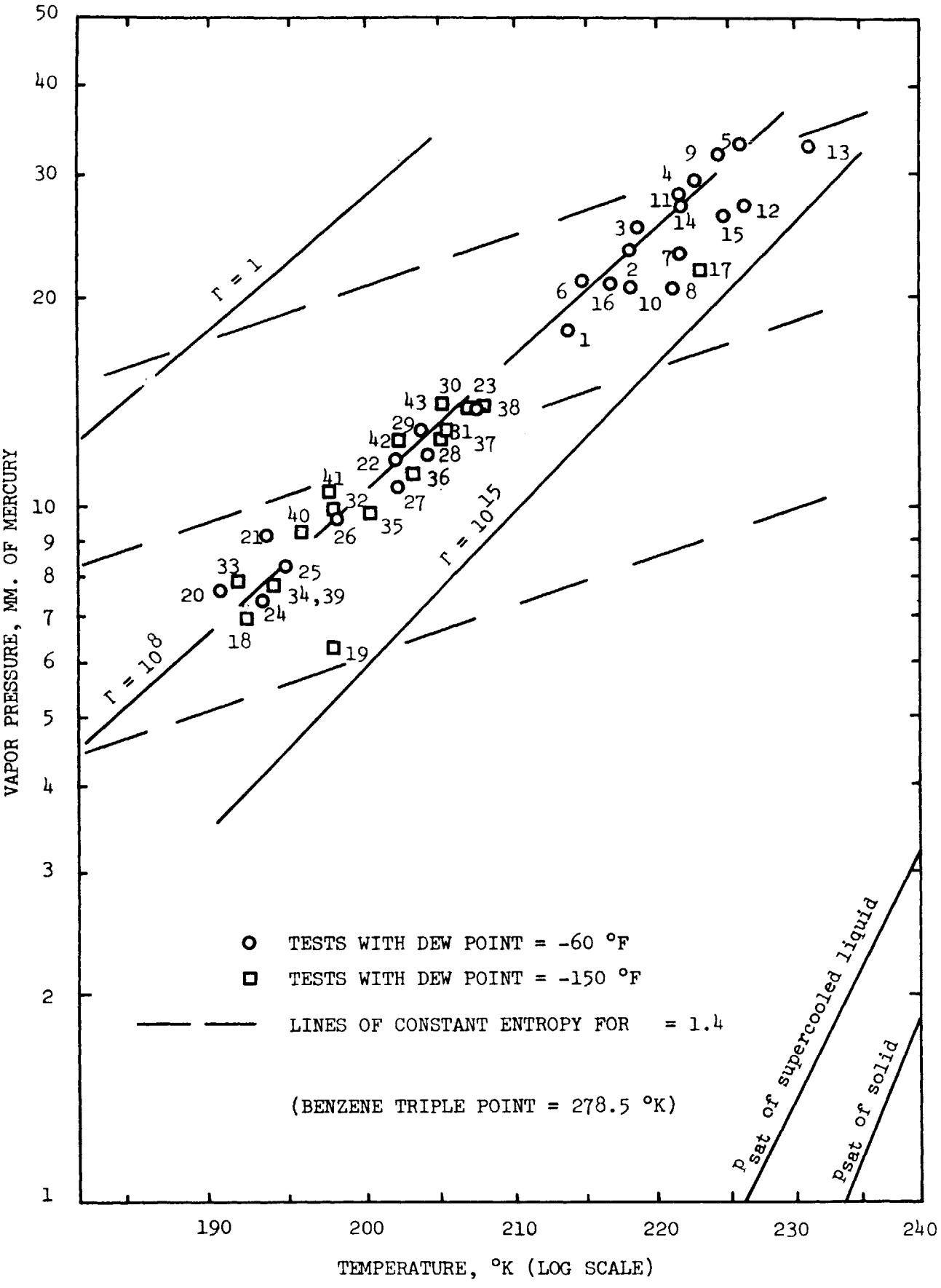

FIGURE 10 MASS-FLOW EFFECT ON PRESSURE PROFILES WITH CHLOROFORM CONDENSATION

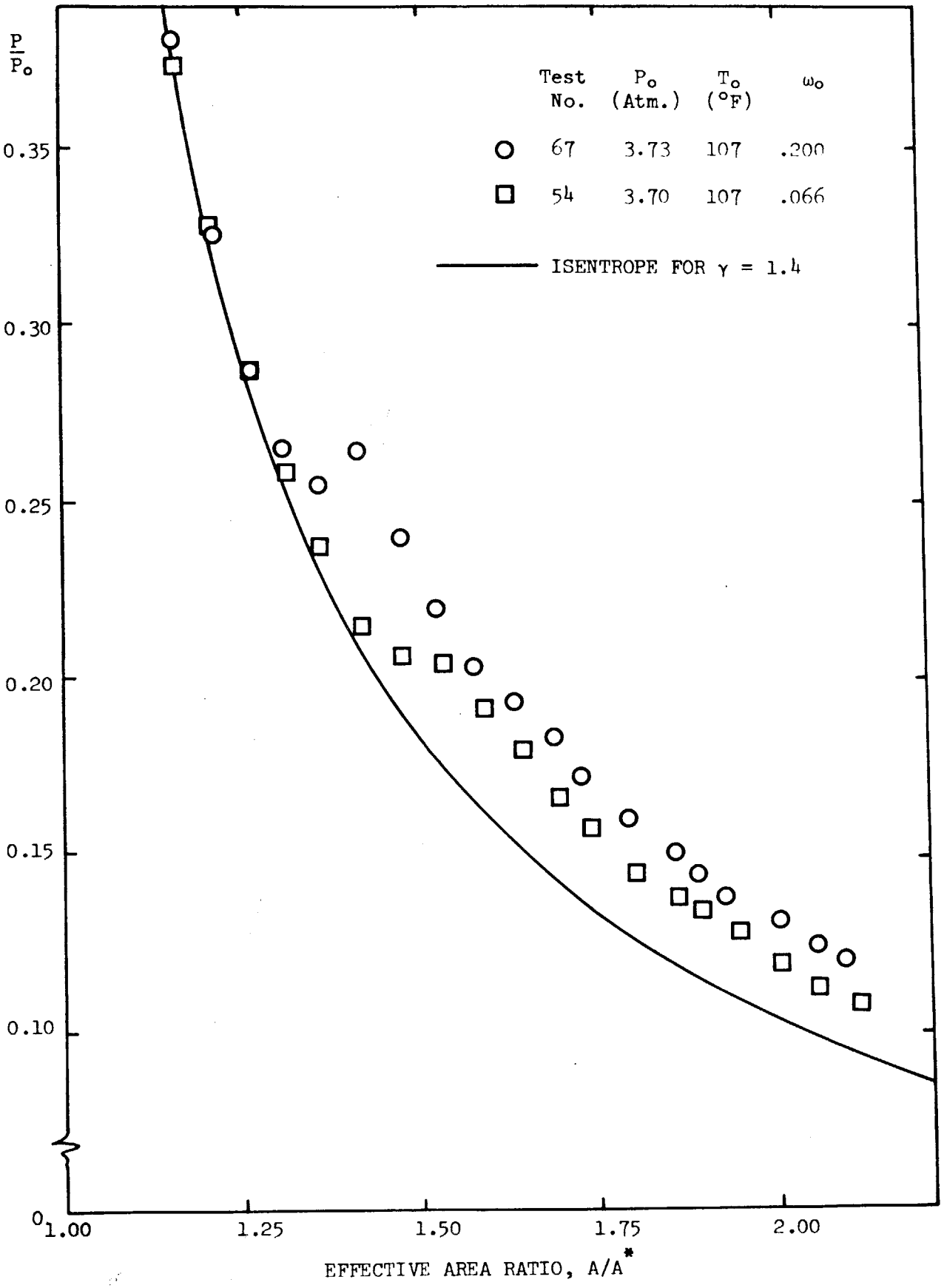

FIGURE 11 TEMPERATURE EFFECT ON PRESSURE PROFILES WITH CHLOROFORM CONDENSATION

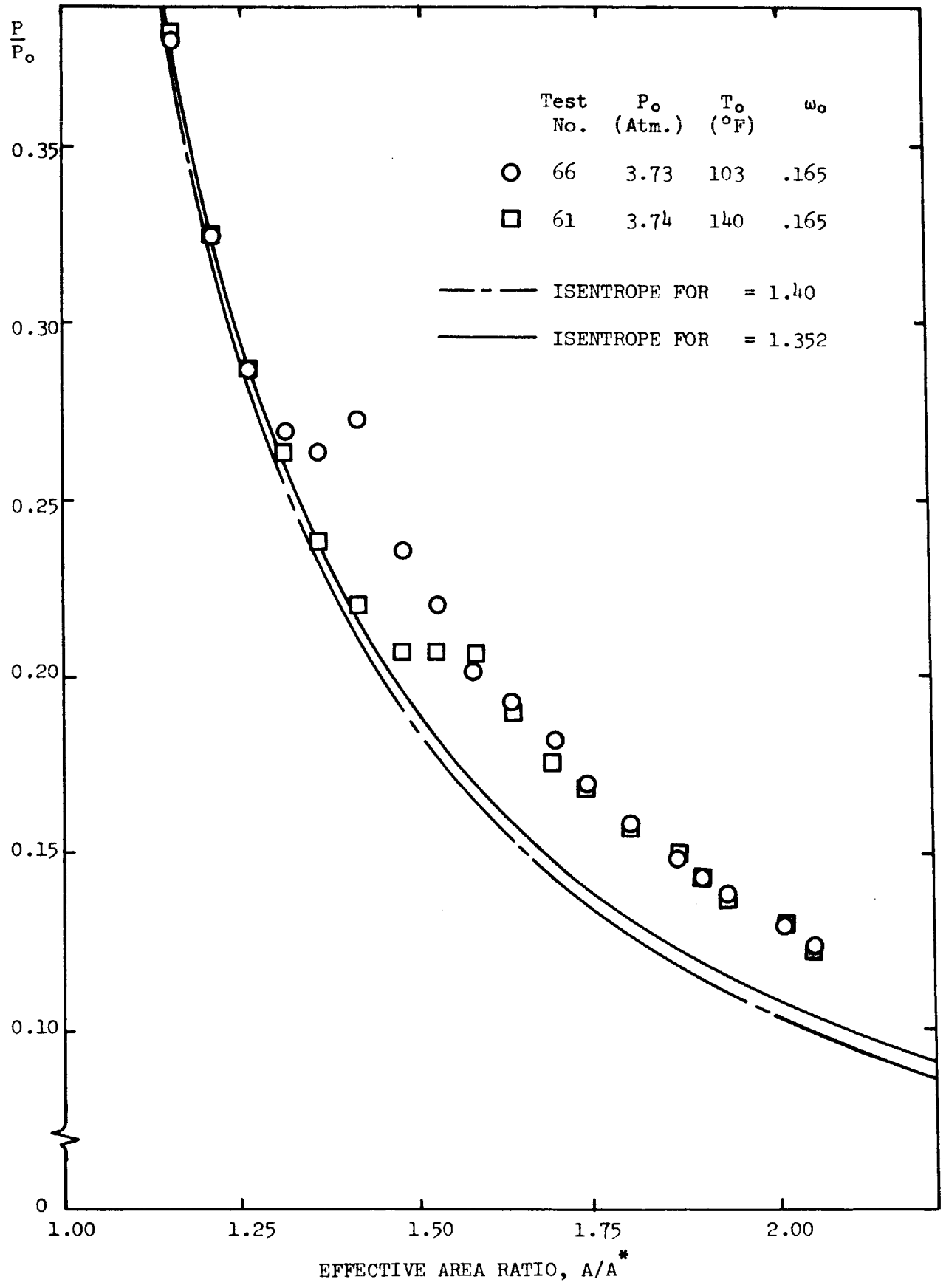

FIGURE 12 COMPARISON OF THEORY WITH DATA FOR CHLOROFORM

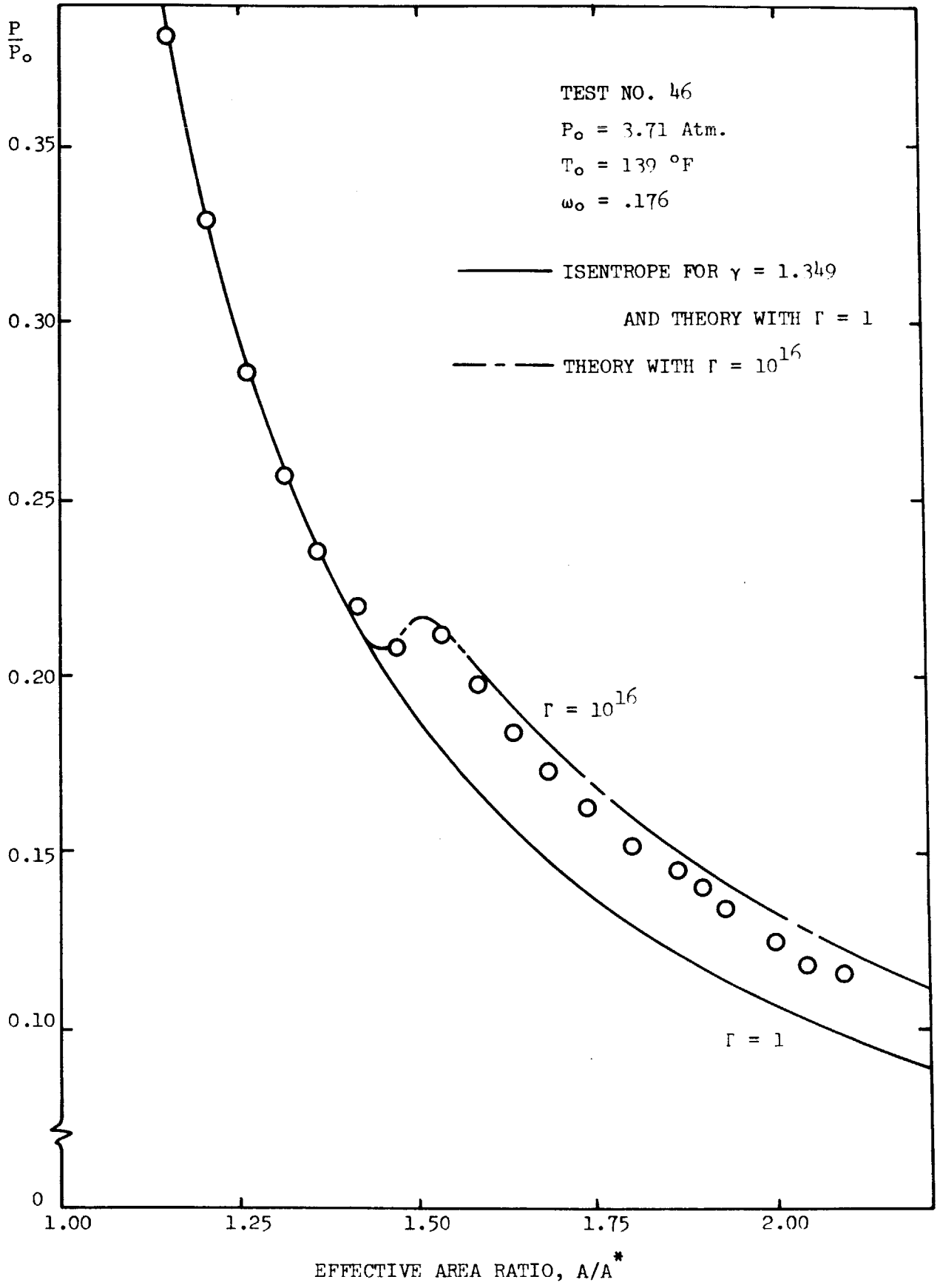

FIGURE 13 COMPARISON OF THEORY WITH DATA FOR CHLOROFORM

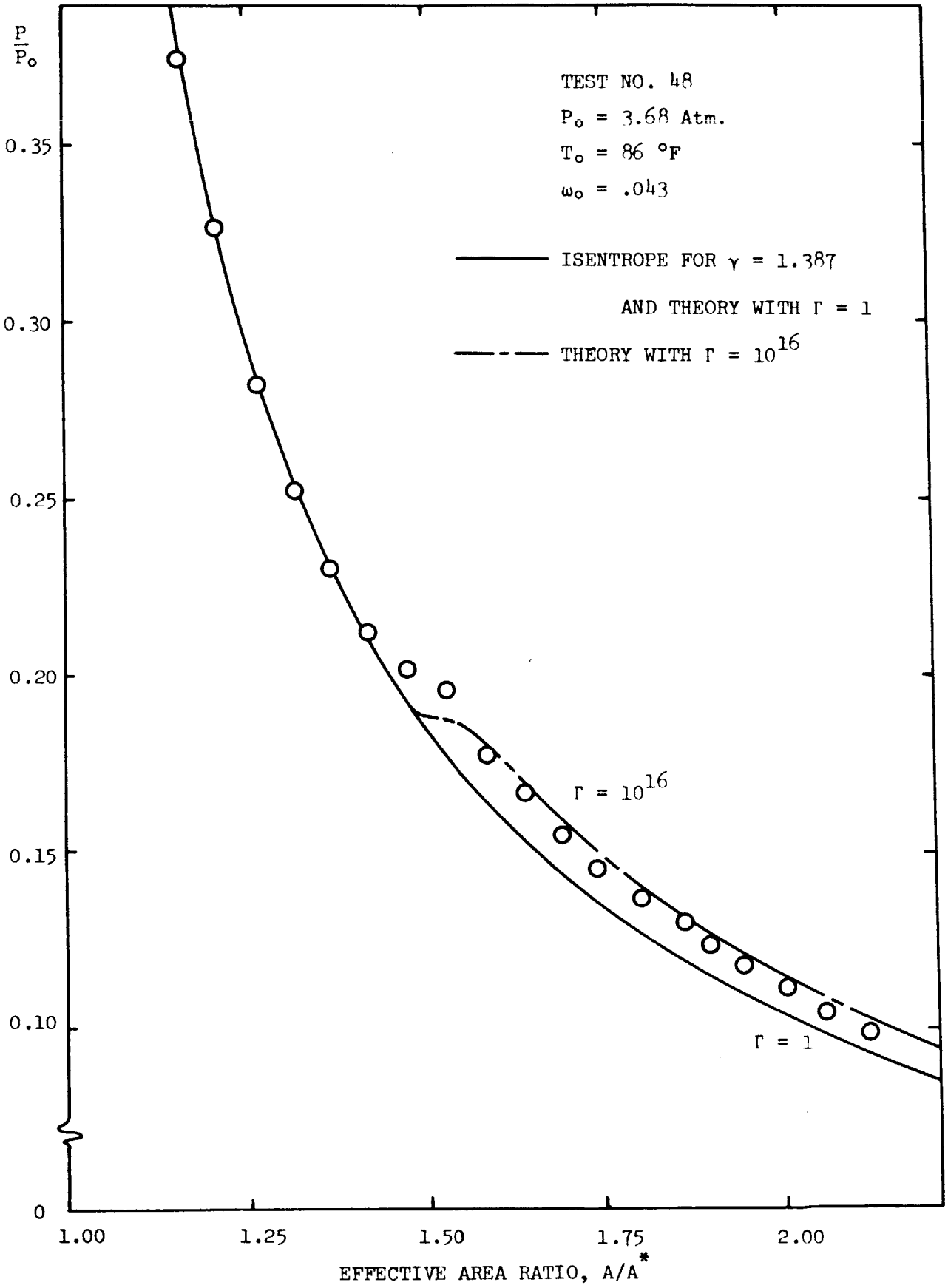

FIGURE 14 COMPARISON OF THEORY WITH DATA FOR CHLOROFORM

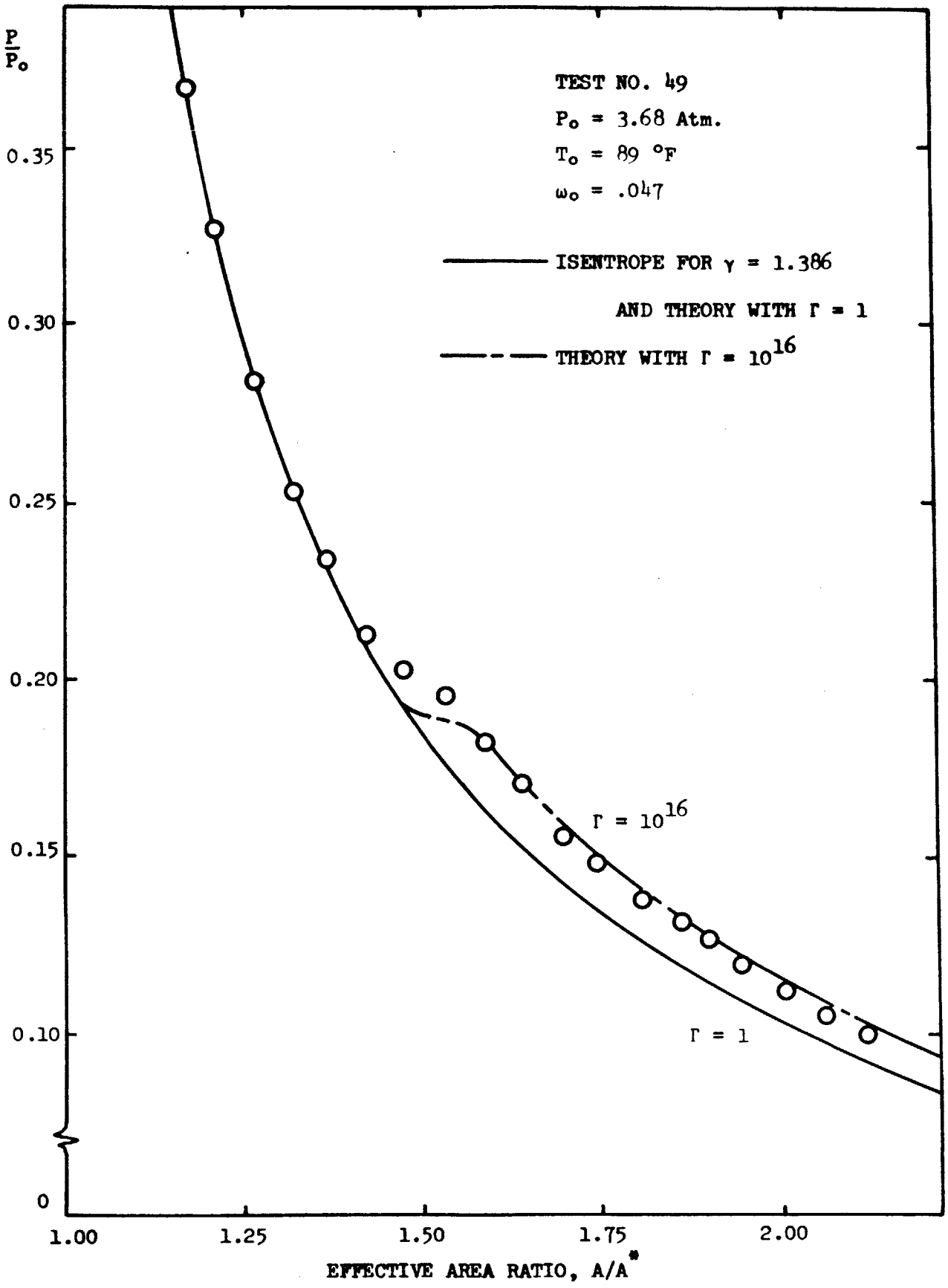

FIGURE 15 INCIDENCE OF CHLOROFORM CONDENSATION